Flexural Behavior of Concrete Using Basalt FRP Rebar

by

Dylan Trotsek

A Thesis Submitted to the Faculty of

The College of Engineering and Computer Science

In Partial Fulfillment of the Requirements for the Degree of

Master of Science

Florida Atlantic University

Boca Raton, FL

August 2017

Flexural Behavior of Concrete Using Basalt FRP Rebar

by

Dylan Trotsek

This thesis was prepared under the direction of the candidate's thesis advisor, Dr. Madasamy Arockiasamy, Department of Civil, Environmental and Geomatics Engineering, and has been approved by the members of his supervisory committee. It was submitted to the faculty of the College of Engineering & Computer Science and was accepted in partial fulfillment of the requirements for the degree of Master of Science.

SUPERVISORY COMMITTEE:
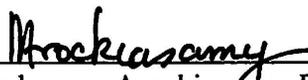
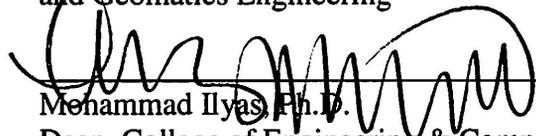Madasamy Arockiasamy, Ph.D. P.Eng., P.E.
Thesis Advisor

Yan Yong, Ph.D.

Sudhagar Nagarajan, Ph.D.

Yan Yong, Ph.D.
Chair, Department of Civil Environmental and Geomatics Engineering

Mohammad Ilyas, Ph.D.
Dean, College of Engineering & Computer Science

Deborah L. Floyd, Ed.D.
Dean, Graduate College

July 27, 2017
Date

iii

ACKNOWLEDGEMENT

ABSTRACT

Author: Dylan L. Trotsek

Title: Flexural Behavior of Concrete Using Basalt FRP Rebar

Institution: Florida Atlantic University

Thesis Advisor: Dr. M. Arockiasamy

Degree: Master of Science

Year: 2017

The objective of this research is to determine if the deflection equations currently adopted in ACI 440.1r-15 and previously ACI 440.1r-06 accurately reflect the flexural behavior of an over-reinforced Basalt Fiber Reinforced Polymer (BFRP) concrete beam. This was accomplished with experimental, analytical and numerical models. The experiment consisted of two beams doubly-reinforced with BFRP rebar. A three-point flexural test on beams with a 30 in. clear span was performed and the deflections were recorded with a dial gauge and LVDT system. This data was compared to the equations from ACI 440.1r-06, ACI 440.1r-15, Branson's equation and a numerical model created in ANSYS Mechanical APDL.

Experimental results show a stiffer beam than expected when compared to the four predictive models for deflection. This can be due to the level of over-reinforcement and the small clear-span to depth ratio. Further research should be conducted to determine the cause for the additional stiffness.

FLEXURAL BEHAVIOR OF CONCRETE USING BASALT FRP REBAR

LIST OF FIGURES

ix

LIST OF TABLES

LIST OF EQUATIONS

1   INTRODUCTION

1.1   Introduction

Traditional reinforced concrete utilizing structural steel has had a wide range of success throughout the world for decades. Generally, it is a very stiff and durable building material that will continue to be used for years to come. However, poor corrosion resistance of reinforced concrete negatively impacts the intended design life. Unless a viable solution is adopted in the industry, the structures in harsh environments will require maintenance and/or replacement. This is especially troublesome for civil infrastructure due to limited infrastructure budgets. A viable and economic solution to corrosion with reinforced concrete can potentially save billions for both public and private sectors. The current trend of the industry is moving towards the adoption of fiber reinforced polymers (FRP) for harsh environments. This study utilizes basalt fiber reinforced polymer rebar (BFRP) as reinforcement for concrete beams. BFRP is cheaper than carbon fiber and has excellent properties in terms of strength and durability. Basalt is also the most abundantly available rock in the earth's crust which could potentially bring costs to a competitive price level in relation to steel.

Current design requirements such as ACI-440.1r-15 provide guidelines for use of FRP rebar as an alternative to steel in reinforced concrete design. This report is continuously updated with additional research results from on-going studies. This research study will compare results from experimental and numerical studies on the behavior of basalt fiber reinforced polymer rebar (BFRP) reinforced concrete beams.

Objectives and Scope:

I.   Review literature, technical manuals and codes

II.   Perform three point bending experiments on two beam specimens up to failure

III.   Analyze the load deflection behavior based on ANSYS numerical model that accounts for cracked sections.

IV.   Compare results of analytical methods, numerical analysis and experimental data with regards to mid-span deflections and crack development

V.   Discuss additional findings and suggest any recommendations for future research to improve current design guidelines

1.2   Significance of Research

The unknowns associated with FRP materials true behavior may very well be limiting the full potentials of these materials for use in structural applications. This research will contribute/add to already published research and the current design methods outlined in ACI-440.1r-15.

2   LITERATURE REVIEW

2.1   Background

Composite materials first gained popularity following World War II when the military and aerospace industries expanded their applications due to the material's high strength and light weight properties as well as the demand for inexpensive materials during a time of rapid economic growth. Expansion of the highway system in the 1950s and 1970s created a need for a durable material that could withstand harsh environments such as those roadways exposed to deicing salt and marine salt. At this time, glass fiber reinforced polymers (GFRP) were considered to be one of the alternative materials. Although the GFRP was largely overlooked, development continued for possible use of FRP as reinforcements. In the past thirty years FRP has been used in bridges, hospitals that require non-metallic reinforcement, chemical storage and even truss structures (ACI 440.1R-06). FRP can be manufactured as pultruded shapes similar to those typical in industries such as beams, rods, channels, tubing and rebar. One of the major obstacles preventing more common use of FRP in design is concerns about behavior and long-term durability. Further investigation of real world applications and research would help quell these concerns to propel these materials into the engineering 'toolbox' in the future.

The public and private sectors worldwide are facing an enormous economic burden due to the devastating effects of corrosion. According to a study entitled "Corrosion Costs and Preventive Strategies in the United States," conducted from 1999 to 2001 by CC Technologies Laboratories, Inc. it is estimated the direct cost of corrosion in the United

States is $276 billion shared across 26 industrial sectors equating to approximately 3.1% of GDP (Koch, Brongers, Thompson, Virmani and Payer, 2002). At the time of the study, it was estimated the direct cost for highways and bridges in particular was $8.3 billion. The continued development and implementation of more durable structures is critical for future savings and extending the design life of such structures. Bridges typically degrade on the underside where saltwater and air create an environment conducive to corrosion initiation. To protect against corrosion there are prescribed minimums for concrete clear cover, crack widths and special concrete mixes to minimize chloride penetration. Although these do aid in protecting the reinforcement, corrosion is inevitable to some extent. The simple solution in these scenarios is to utilize an FRP rebar as an alternative to structural steel in future designs and construction. The higher initial material costs for these materials can be recognized in the reduction of maintenance and monitoring costs as well as potentially longer life spans.

The most common types of FRP rebar are made from continuous fibers of either aramids (AFRP), basalt (BFRP), carbon (CFRP), or glass (GFRP). FRP reinforcing bars are anisotropic and consist of fibers made from the respective material and a resin matrix. The fibers are typically arranged in a longitudinal direction to utilize the high tensile strength of the materials. These fibers provide stiffness and strength to composite materials and have a major influence on the mechanical properties of the rebar. Therefore, the mechanical properties of the material used to create the fibers will be evident in the mechanical behavior of the composite. The resin matrix protects the fibers and is used to bond the fibers together which uniformly transfers stresses between them and between the FRP rebar and concrete. Due to the complex structure of FRP rebar, long term durability

is not as simple as steel corrosion because degradation can occur in the resin or fibers and their interface bond behavior (Ceroni, Cosenza, Gaetano, Pecce 2006).

This research uses Basalt Fiber Reinforced Polymer (BFRP) rebar as reinforcement in concrete. Basalt fibers are created by melting basalt rock which is a natural inorganic material originating from volcanic lava at 1400 ºC. The fiber is environmentally and ecologically harmless and free from carcinogens and other harmful materials that may cause health issues. It can perform at temperatures ranging between -269ºC and 700ºC. Basalt fibers have high strength and resistance to UV light, acids and corrosion (Elgabbas, Ahmed, and Benmokrane, 2017). These properties make basalt a very durable material that can be used for applications in extreme and harsh environments.

2.2 Comparison of Structural Steel to FRP Materials

2.2.1 Stress-Strain Curves

Steel is a ductile material with a high tensile strength compared to plain concrete which is a brittle material. This ductile failure is important in that it provides ample warning before total failure and depending on the magnitude of failure a structure may exhibit structural integrity to prevent total collapse. As shown in the stress-strain curve for steel in Figure 2-1 (Berkeley.edu), steel has an elastic limit, followed by the yield plateau and then the strain hardening region before reaching the ultimate limit. Most design applications prefer a ductile failure mode which consequently requires a lower factor of safety than more brittle behavior. This can save material and labor costs and provide sufficient warning before failure.

Basalt exhibits exceptional material properties that make it more suitable for harsh environments. However, BFRP as well as other FRP's have properties with limited

ultimate strains. Most importantly, BFRP does not possess such a distinct stress-strain curve as that of steel. Based on uniaxial tensile tests on five similar BFRP rebar, Fan and Zhang (2016), observed that after an initial linear elastic region there is a very small hardening region followed by ultimate failure. This hardening region is typically not considered in design or deflection computations. Results from these experiments in Figure 2-2 show the magnitude of the linear elastic region up until brittle failure. This justifies the assumption that this material is 'linear elastic'. Unfortunately, this type of brittle failure is dangerous because there is little or no warning before a catastrophic collapse. Due to this failure mode, ACI 440.1r-15 recommends a higher factor of safety which is realized with smaller reduction factors as shown in Equation 1.

Alternatively to normal reinforced concrete design, concrete crushing is considered to be a safer failure mechanism since the FRP reinforcement will maintain some strength to resist load without complete collapse. This is the reasoning for increasing reduction factors as the reinforcement ratio increases. Since actual concrete strength may be greater than specified strengths, a designed over-reinforced member may still cause failure in the FRP reinforcement. To account for this issue, a member is not considered to be over-reinforced until the reinforcement ratio is greater than or equal to 1.4 times the balanced ratio ($\rho_f \geq 1.4\rho_{fb}$).

Equation 1 Reduction Factors Based on Reinforcement Ratio (ACI 440.1r-15)

$$\varphi = \begin{cases} 0.55 \ for \ \rho_f \leq \ \rho_{fb} \\ 0.3 + 0.25\dfrac{\rho_f}{\rho_{fb}} \ for \ \rho_{fb} < \ \rho_f < 1.4\rho_{fb} \\ 0.65 \ for \ \rho_f \ \geq \ 1.4\rho_{fb} \end{cases}$$

Another obstacle during member design phase is that the low modulus of elasticity (6.6×10^6 psi for #2 rebar) of BFRP will cause excessive deflections when compared to

similar steel reinforced concrete beams. Figure 2-3 shows a comparison of the modulus of elasticity for different types of FRP compared to steel based on the average tensile strength and modulus of elasticity from ACI-440.1r-15 and manufacturer provided specifications. Steel yielding is not considered in this graphic. It is apparent that aside from CFRP, the other types of FRP show significantly greater strain at the same stress when compared to steel due to the lower modulus of elasticity. Since serviceability limit states control many designs with FRP this directly affects the overall beam design even if the nominal moment capacity of the BFRP beam is larger than a traditional steel reinforced beam.
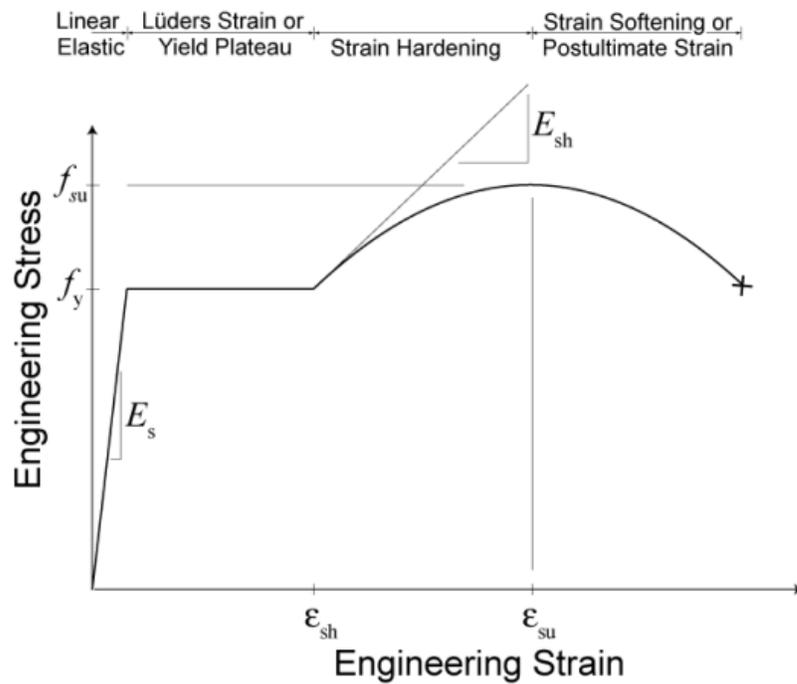
Figure 2-1 Stress-Strain Curve for Steel (Source: Berkeley.edu)

7
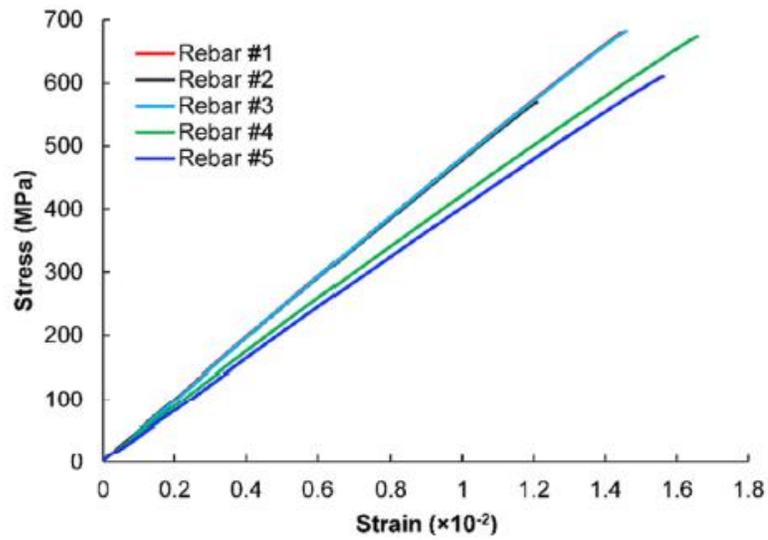
Figure 2-2 Stress-Strain Curve Obtained from Uniaxial Tensile Tests of BFRP Rebar (Fan and Zhang 2016)
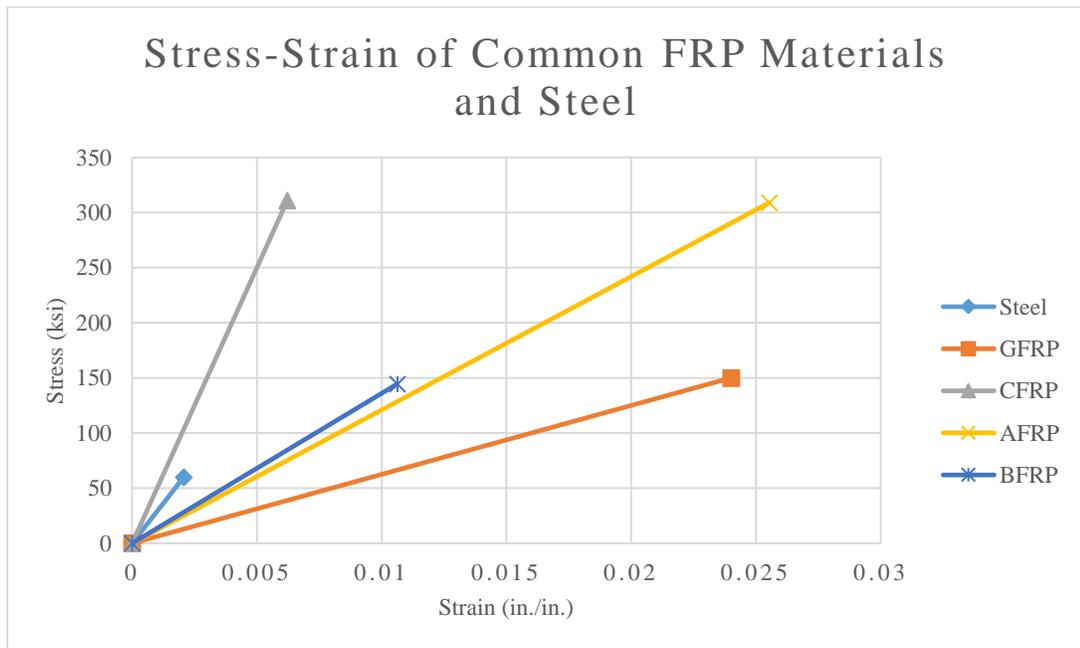
Figure 2-3 Stress-Strain Relationship of Various FRP Materials Compared to Steel

2.2.2   Material Strength

The steel rebars manufactured are: Gr. 40 (f_y=40 ksi), Gr. 60 (f_y=60 ksi) and Gr. 75 (f_y=75 ksi). For purposes of reinforced concrete design only the yield strength is utilized for tension and compression capacity. For steel used strictly as shear reinforcement the shear strength is typically taken as 0.6 f_y. The ability for steel to provide high strengths in multiple directions make steel superior when compared to many FRP rebars.

BFRP as well as other FRP rebar are manufactured in a manner that they are used primarily as tensile reinforcement. BFRP has exceptional tensile properties with a yield strength of 127 ksi for #2 rebar and 80 ksi for #10 rebar per manufacturer (Smarter Building Systems) Table 2-1. Comparison of the most common FRP materials and steel are shown in Table 2-2 (ACI-440.1r-15) with BFRP data provided by the manufacturer. Some manufacturers will use hollow sections for larger size rebar which would adversely affect the nominal area. ACI 440.1r-15 does not recommend consideration of any contribution of FRP rebar in compression. Based on research by Wu (1990) it was determined that compressive strengths varied from 20-78 percent of the tensile strength for GFRP, CFRP and AFRP. There are no current standard test methods to characterize compressive strength and values should be obtained from the manufacturer when necessary. Shear strength of FRP is dependent on the orientation of fibers. Placing them in an off-axis direction will increase shear strength (ACI 440.1r-15). Similar to compression strength, shear strengths should be obtained from the manufacturers.

Table 2-1 Strength Properties of BFRP Rebar (Smarter Building Systems)

Rebar Size	Diameter (in)	Tensile Strength (ksi)	Tensile Modulus of Elasticity (ksi)
2	0.250	127	6686.24
3	0.375	123	6700.74
4	0.500	115	6729.75
5	0.625	99	6990.82
6	0.750	95	6903.80
7	0.875	91	6729.75
8	1.000	89	7396.92
10	1.270	80	6091.58

Table 2-2 Comparison of Tensile Properties of Common FRP Materials and Steel

	Steel	GFRP	CFRP	AFRP	BFRP*
Nominal yield stress, ksi	40-75	NA	NA	NA	NA
Tensile strength, ksi	70-100	70-230	87-535	250-368	101-188
Elastic modulus, 10^3 ksi	29	5.1-7.4	15.9-84.0	6.0-18.2	6.2-9.4

Information provided by rebar manufacturer (Smarter Building Systems

2.3   Design and Research of BFRP Beam Behavior

2.3.1   Code Adoption for Crack Control

Controlling of crack widths in steel reinforced concrete is for both aesthetics and to maintain the protective concrete cover to limit degradation of the reinforcement from the surrounding environment. Two methods presently exist for determining reinforcement requirements to limit flexural cracking in steel reinforced concrete; the direct and indirect procedures. The direct procedure (empirical model) calculates crack widths for a particular member which are then compared to the allowable crack widths. ACI 318-99 replaced the traditional direct method and z-factor with the indirect procedure. The indirect procedure (physical model) controls cracking based on center-to-center spacing of reinforcement which is then compared to the preferred crack width as shown in Equation 2. ACI 318 Section 10.6.4 crack control provisions for steel reinforcement limits crack widths to between 0.018 and 0.022 in.

Equation 2 Bar Spacing for Beams and One-way Slabs:

$$s = 15\left(\frac{40{,}000)}{f_s}\right) - 2.5c_c < 12\left(\frac{40{,}000)}{f_s}\right)$$

$s = center-to-center\ spacing\ of\ tensile\ reinforcement\ (in.)$

$c_c = concrete\ clear\ cover\ (in.)$

$f_s = stress\ in\ reinforcement\ (psi)\ (can\ be\ taken\ as\ \frac{2}{3}f_y\ for\ service\ load)$

FRP materials are non-corrosive and generally more resistant to harsh environments. Therefore, crack widths that are limited for corrosion protection do not necessarily need to adhere to such stringent crack width limits when designing with these reinforcements. As previously discussed, the lower modulus of elasticity for FRP rebar will cause additional

11

concrete cracking at the same stress. ACI 440.1r-15 recommends an alternative to determining maximum bar spacing (Equation 3). This equation accounts for stiffness of reinforcement, a maximum crack width, and the bond between the FRP and concrete. These values must also comply with Equation 4 for clear spacing. ACI recommends maintaining crack widths between 0.016 in. and 0.028 in. when crack control is necessary for aesthetic purposes.

Equation 3 ACI 440.1r-15 Bar Spacing:

$$s_{max} = 1.15 \frac{E_f w}{f_{fs} k_b} - 2.5c_c \le 0.92 \frac{E_f w}{f_{fs} k_b}$$

$s_{max} = center - to - center\ spacing\ of\ tensile\ reinforcement\ (in.)$

$\quad E_f = guaranted\ modulus\ of\ elasticty\ of\ FRB\ rebar\ (psi)$

$\quad f_{fs} = stress\ in\ reinforcement\ (psi)\ (service\ load\ for\ design\ purposes)$

$\quad k_b = bond - dependend\ coefficient\ (assumed\ 1.0)$

$\quad w = design\ crack\ width\ (in.)$

$c_c = concrete\ clear\ cover\ (in.)$

Equation 4 Minimum Distance from Extreme Tensile Fiber and Center of Tensile Reinforcement:

$$d_c \le 0.92 \frac{E_f w}{2 f_{fs} \beta k_b}$$

$d_c = distance\ of extreme\ tensile\ fiber\ to\ center of\ tensile\ reinforcement\ (in.)$

$\quad E_f = guaranteed\ modulus\ of\ elasiticty\ of\ FRB\ rebar\ (psi)$

$\quad f_{fs} = stress\ in\ reinforcement\ (psi)\ (service\ load\ for\ design\ purposes)$

$k_b = bond - dependend\ coefficient\ (assumed\ 1.0)$

$w = design\ crack\ width\ (in.)$

$\beta = ratio\ of\ distance\ from\ neutral\ axis\ to\ center\ of\ tensile\ reinforcement$

2.3.2   Research on Crack Development and Behavior

Research on crack propagation of BFRP concrete was conducted by Urbanski, Lapko and Suprynowicz (2015). Beams made with steel reinforcement were compared to beams made of BFRP reinforcement at the same reinforcement ratios ranging from 0.5%-1.99%. A three point flexural test was performed on each beam and the crack propagation in the constant bending moment region was recorded with a Digital Image Correlation (DIC) System. Output from this system is shown in Figure 2-4 which clearly displays fewer, but wider cracks developing in the BFRP reinforced beams. Larger crack spacing in the BFRP can be associated with the lower modulus of the BFRP which allows it to maintain an adequate bond with the concrete whereas the stiff steel does not undergo the same strain as the concrete causing a breakdown of the bond between the steel and concrete. Results of the experiment (Table 2-3) show BFRP beams consistently developing much wider cracks and spacing as opposed to their steel reinforced counterparts.
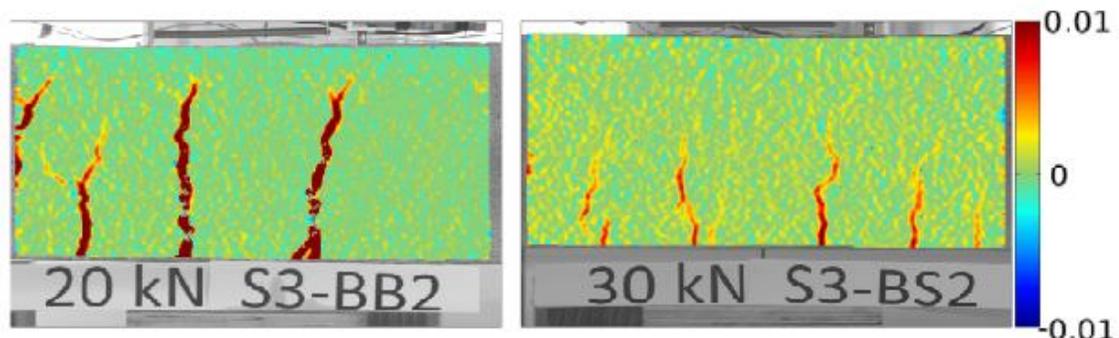
Figure 2-4 DIC Showing Significant Crack Width Development of BFRP Reinforced Beam (Left) vs. Steel Reinforced Beam (Right) [Urbanski, Lapko and Suprynowicz (2015)]

13

Table 2-3 Mean (w_m), Minimum (w_{min}) and Maximum (w_{max}) Crack Width Development in BFRP and Steel

Beams of Equal Reinforcement Ratios,(Urbanski, Lapko & Suprynowicz, 2015))

Beam description	w_m [mm]		w_{min} [mm]		w_{max} [mm]		w_{min}/w_m		w_{max}/w_m	
	BFRP	Steel	BFRP	Steel	BFRP	Steel	BFRP	Steel	BFRP	Steel
S1-B1	0.80	0.04	0.30	0.03	1.30	0.05	0.38	0.75	1.63	1.25
S1-B2	0.87	0.05	0.40	0.03	2.00	0.05	0.46	0.60	2.30	1.00
S2-B1	0.42	0.05	0.10	0.03	0.70	0.10	0.24	0.60	1.67	2.00
S2-B2	0.88	0.06	0.10	0.05	1.70	0.10	0.11	0.83	1.93	1.67
S3-B1	0.51	0.05	0.05	0.03	1.00	0.10	0.10	0.60	1.96	2.00
S3-B2	0.44	0.07	0.05	0.05	0.80	0.10	0.11	0.71	1.82	1.43
$w_{average}$	0.65	0.05	0.17	0.04	1.25	0.08	0.23	0.68	1.89	1.56

The experiment performed by Elgabbas, Vincent, Ahmed & Benmokrane (2016) aimed at determining the bond-dependent coefficient (k_b). Crack development was noted during the experiment in order to determine this coefficient. The experimentally derived bond-dependent coefficient was 0.76±0.03 for sand-coated BFRP which is smaller than the value of 1.4 adopted by ACI 440.1r-15. Reinforcement ratios for the beams used in the experiment are shown in Table 2-4. Similar to experiments performed by Urbanski, Lapko and Suprynowicz (2015) there was a correlation between reinforcement ratio and crack width and distribution (Table 2-5). The recommended k_b value per ACI 440.1r-15 overestimated crack widths by 34%.

Table 2-4 Reinforcement Ratios for Beams

Beam ID[a]	ρ_f	ACI [3]	
		ρ_{fb} [b]	ρ_f/ρ_{fb}
B-2#10 mm	0.0030	0.0023	1.35
B-4#10 mm	0.0060	0.0023	2.89
B-2#12 mm	0.0043	0.0024	1.83
B-4#12 mm	0.0086	0.0024	3.95
B-2#16 mm	0.0077	0.0025	3.13
B-4#16 mm	0.0154	0.0025	6.81

Table 2-5 Determination of Bond-Dependent Coefficient Based on Average from Three

First Cracks (Elgabbas, Vincent, Ahmed & Benmokrane, 2015)

Beam	Crack #1	Crack #2	Crack #3	Average
B-2#10 mm	0.82	0.79	0.71	0.77
B-4#10 mm	0.59	1.02	0.68	0.76
B-2#12 mm	1.14	0.46	0.75	0.78
B-4#12 mm	0.65	0.73	0.77	0.72
B-2#16 mm	0.67	0.66	0.91	0.75
B-4#16 mm	0.57	0.66	1.17	0.80
Average				0.76
Standard deviation				0.03

2.3.3   Deflection Criteria

2.3.3.1   Development of Code Deflection Criteria

Serviceability requirements limit deflection based on length of member and its intended use. Determination of deflection is a function of load and stiffness along a member. With a member such as a steel beam the gross moment of inertia (I_g) should not change throughout its lifespan as long as the member remains in the elastic range without any cracks. Unlike steel, reinforced concrete is brittle and inherently cracks after reaching

the cracking moment when tension stresses in the concrete exceed the modulus of rupture. Depending on requirements of a member it is possible that a reinforced concrete member has cracks during its service life that reduce the effective moment of inertia. It is important to have an accurate model to accurately calculate deflections at various loads   based on the effective moment of inertia (I_e) .

Crack propagation continues with increase in load after first crack until failure occurs. To account for this change in the effective moment of inertia, ACI 318-11 recommends the use of Branson's Equation (Equation 5) to determine the deflection throughout the loading of a member. This equation considers the gross moment of inertia, cracked moment of inertia, cracking moment and the applied moment to determine an effective moment of inertia at any applied load. A linear-elastic behavior in a reinforced concrete beam will continue until the external moment reaches the cracking moment value at first crack. After the first cracking moment this equation provides a transition between the gross moment of inertia and the cracked moment of inertia based on the ratio of the cracking moment and applied moment up until ultimate load. The variable m can be taken as 4 to determine the effective stiffness at a section or taken as 3 for the average stiffness over the entire span (Bishoff, 2005). Since the average stiffness along the span is of more concern it is typical to use a value of m set equal to 3. Overall deflection behavior throughout various loading cycles is possible by determining the effective moment of inertia for each successive applied moment which is substituted for the maximum service moment (M_a) during each iteration.

Equation 5 Branson's Equation for Effective Moment of Inertia (ACI 318-11):

$$I_e = \left(\frac{M_{cr}}{M_a}\right)^m I_g + [1 - \left(\frac{M_{cr}}{M_a}\right)^m]I_{cr} \leq I_g$$

Where

Equation 6 Cracking Moment

$$M_{cr} = \frac{f_r I_g}{y_t}$$

and

Equation 7 Modulus of Rupture

$$f_r = 7.5\lambda\sqrt{f'_c}$$

With

$I_e = effective\ moment\ of\ inertia\ (in.^4)$

$I_g = gross\ moment\ of\ inertia\ (in.^4)$

$I_{cr} = moment\ of\ inertia\ of\ transformed\ section\ (in.^4)$

$M_{cr} = cracking\ moment\ of\ inertia\ (lb - in.)$

$M_a = maximum\ service\ load\ of\ member\ (lb - in.)$

$f_r = modulus\ of\ rupture\ (psi)$

$f'_c = specified\ concrete\ compressive\ strength\ (psi)$

$y_t = distance\ from\ centroidal\ axis\ of\ gross\ section\ to\ tension\ face\ (in.)$

$\lambda = modification\ factor\ for\ lightweight\ concrete$

The original Branson's equation for steel reinforced concrete did not translate into an accurate model for FRP reinforced concrete. Research on deflection of FRP-reinforced concrete beams has shown that Branson's equation underestimates deflection as the gross-to-cracked moment stiffness I_g/I_c approached 3 to 4 (Nawy & and Neuwerth 1977; Benmokrane et al. 1996; Yost et al. 2003 cited in ACI 440-1r.15). This model for the

effective moment inertia was correlated to steel reinforced concrete beams with a gross-to-cracked moment of inertia ratio from 1 to 4 (Bischoff 2005). This empirical model fails to correctly account for tensile stresses in concrete between cracks. FRP members may have a cracked-to-uncracked moment of inertia ratio from three to five times that of traditional steel reinforced members which will affect the tension stiffening when compared to those beams that were used to model the formulation. This causes the model to provide unrealistic stiffness values (Bischoff 2005).

Presented in ACI 440-1r.06, a modification factor was included in Branson's equation which was originally proposed by Gao, et al. (1998a cited in ACI 400-1r-06) as shown in Equation 8. As previously noted, the original equation overestimated the effective moment of inertia for cracked beams which could imply that tension stiffening was not occurring to the same extent as a traditional reinforced concrete beam. To account for the lesser degree of tension stiffening, the modification factor β was included in the modified Branson's equation.

Equation 8 Modified Branson's Equation (ACI 440.1r-06)

$$I_e = \left(\frac{M_{cr}}{M_a}\right)^3 \beta I_g + [1 - \left(\frac{M_{cr}}{M_a}\right)^3]I_{cr} \leq I_g$$

Where

$$\beta = \frac{1}{5}\left(\frac{\rho_f}{\rho_{fb}}\right) \leq 1.0$$

This modified Branson's equation was replaced with a modification of Bischoff's proposed equation in ACI 440.1r-15. This equation is a version of the section-based method proposed by Bischoff (2005). The modified version of this equation known as the

Bischoff's Section-based equation (Equation 9) represents the weighted average of the flexibility ($1/E_cI$) as opposed to the original Branson equation which represents a weighted average of stiffness (E_cI). There is a modification factor γ that accounts for the variation of stiffness along the member with consideration to the length of the uncracked regions and the change in stiffness in the cracked regions. Determination of this factor is also dependent on the load and boundary conditions. The recommended equation for γ, representing a simply supported beam with uniformly distributed load applied is shown in Equation 9. This expression requires γ to be recalculated every iteration due to the inclusion of the applied moment.

Equation 9 Bischoff's Section-based expression (ACI 440.1r-15)

$$I_e = \frac{I_{cr}}{1 - \gamma \left(\frac{M_{cr}}{M_a}\right)^2 \left(1 - \frac{I_{cr}}{I_g}\right)} \leq I_g; \ M_a \geq M_{cr}$$

Where

$$\gamma = 1.72 - 0.72 \left(\frac{M_{cr}}{M_a}\right)$$

2.3.3.2   Research of Code Criteria

Many experiments have been performed focusing on the deflection of BFRP beams. Prior to 2015 the modified Branson's equation was solely adopted by ACI 440. In an experiment conducted by Zhang, Sun & Xiong (2013), data was collected from numerous experiments composing of 91 concrete beams. The experimental deflections were compared to the results based on modified Branson's equation. Comparisons between predicted and experimental results, $\delta_{pred}/\delta_{exp}$ for $0.3M_u$ and $0.5M_u$, $0.7M_u$ and M_u were in the range of approximately 0.8. The highest standard deviation was 0.4 noted at $0.3M_u$

which then tapered off to less than 0.2 at M_u. Overall, the modified Branson equation underestimated the experimental deflections throughout all loading stages.

BFRP reinforced concrete beams were also examined by Lapko & Urbanski (2015). In this experiment the deflections of three BFRP beams were compared to the modified Branson equation (ACI-440.1r-06 adoption), and the modified Bischoff equation proposed by Bischoff and Gross (2011) that has been adopted by ACI 440.1r-15. Results of the predicted and experimental deflections are shown in Table 2-6. Up to the stage of 20-30% of critical load, Bischoff's Section-based Method more accurately estimated the experimental deflections. Both equations underestimated the experimental deflections. Into the 40-60% of critical load, both equations were similar amongst the other equations investigated in this research and correctly or overestimated deflection. At over 72% of the critical load the results from both equations were similar and the values from other equations underestimated the deflection.

Table 2-6 Results of Predicted and Experimental Deflections

Stage of Loading	Predicted vs. Experimental Deflections	
	Modified Branson (ACI 440.1r-06)	Bischoff's Section Based Method (ACI 440.1r-15)
After First Crack	up to 87% underestimation	34% underestimation
20-30% Critical Load	36% underestimation	3% underestimation
40-60% Critical Load	1-15% overestimation	1-15% overestimation
Over 72% Critical Load	12-30% underestimation	12-30% underestimation

The research conducted by Elgabbas, Vincent, Ahmed & Benmokrane (2015) investigated deflection response in addition to the crack propagation. It was evident that deflections were very similar between the various reinforcement ratios of the beams up until the predicted cracking moment. Similarly, higher reinforcement ratios had higher post-cracking stiffness until failure. At $0.30M_n$, results indicate the modified Branson equation

underestimated mid-span deflection with $\delta_{exp}/\delta_{pred}$ equal to 2.10 ± 0.37. At $0.67M_n$ there is an underestimation of deflection with $\delta_{exp}/\delta_{pred}$ equal to 1.08 ± 0.04. In comparison Bischoff's Section-based Method had an average $\delta_{exp}/\delta_{pred}$ equal to 1.35 ± 0.15 and 1.03 ± 0.05 at $0.30M_n$ and $0.67M_n$ respectively. This shows a more distinct difference in accuracy of both equations as opposed to Lapko & Urbanski (2015) that did not have such clearly defined difference after $0.30M_n$. Additionally, results from this experiment did not show an overestimation of deflection.

There were apparent disparities between experimental and predicted results with the modified Branson's method and Bischoff's section based method. It appears through reviewed research that there is an improvement in deflection predictions using Bischoff's section based method. This is expected since this is the most recently adopted equation in ACI 440.1r-15. There seems to be a lack of information regarding the accuracy of the equations adopted by ACI 440.1r-15.

3   BFRP REINFORCED CONCRETE BEAM DESIGN AND EXPERIMENTAL

SETUP

3.1   BFRP Reinforced Concrete Beam Design

Taking into consideration of experimental equipment limits, the beam size was chosen to be 7" x 4" x 33" with dimensions larger than the standard ASTM specimen size in cross section and length (6 x 6 x 18 in.). Tensile reinforcement consisted of two #3 BFRP rebar with a yield strength, f_y=123 ksi spaced 1.875" center-on-center. This provides a reinforcement ratio (ρ) equal to 0.0093 which is greater than the balanced ratio (ρ_{fb}) of 0.0043. As recommended by ACI-440.1r-15 this beam is over-reinforced which does not develop the full reinforcement capacity after concrete crushing. Two more #3 BFRP rebar were utilized as stirrup hangers at the top of beam. The beam was designed to prevent premature shear failure of beam. Three stirrups made of Grainger 0.25" threaded rods with a yield strength, f_y=45 ksi were provided near the end zones at the two supports. The first stirrup was positioned with a 2" spacing from the support and the subsequent stirrup spacing was 3.5". A concrete clear cover of 0.625" was maintained around all four sides of the beam. Figure 3-1 shows the cross-sectional details for the two beam specimens. The side view of the beam showing the spacing of shear stirrups is shown in Figure 3-2. Forms were built using 7/8" plywood and are shown in Figure 3-3. Canola oil was applied as a form release agent a day prior to pouring concrete. Excess canola oil was removed using paper towel.
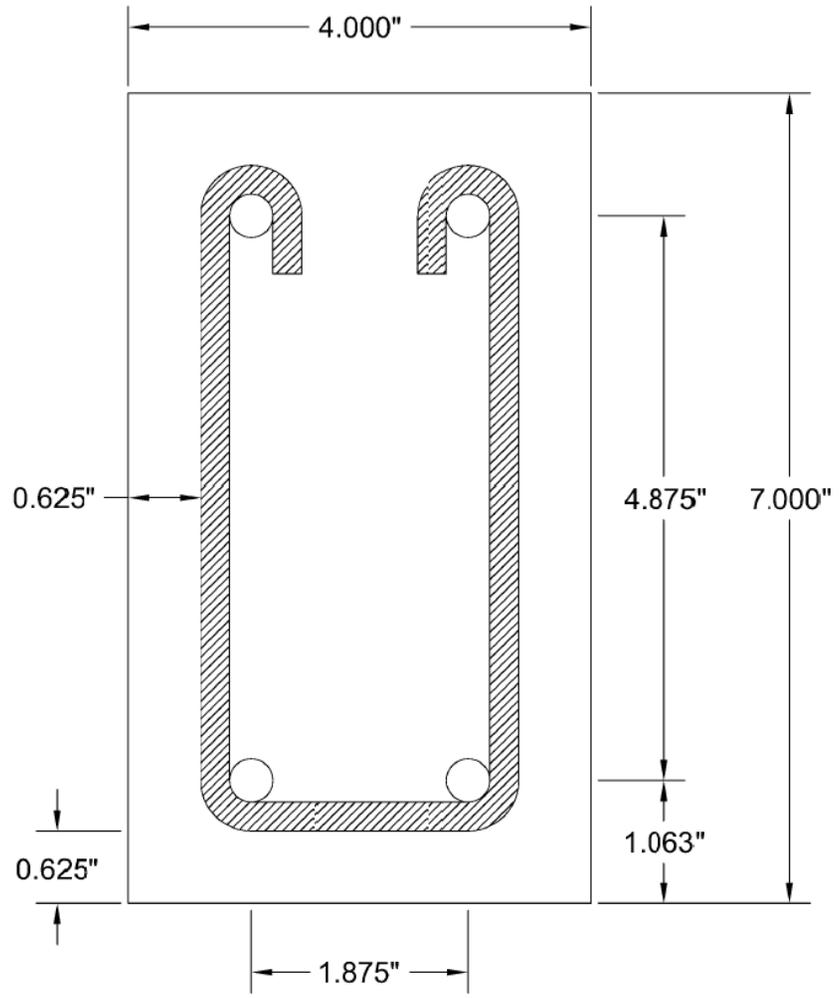
Figure 3-1 Cross-Section of Beam Specimen
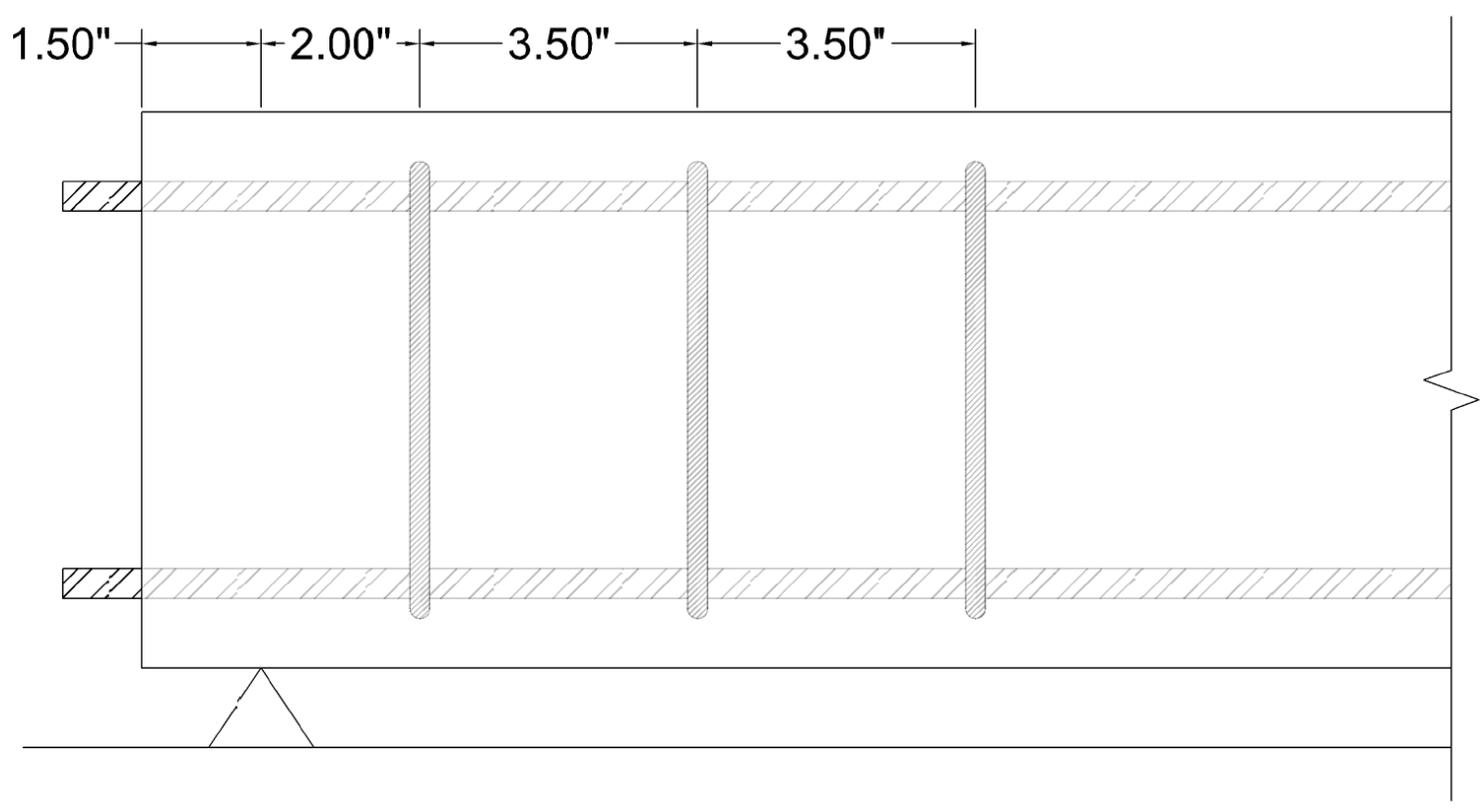
Figure 3-2 Side View of Beam

Figure 3-3 BFRP Reinforcemnts Positioned in Plywood Forms

A concrete mix with a design strength of $f'_c =$ of 5000 psi was used to limit the moment capacity of the beam. In order to achieve this compressive strength, the mix design used a water to cement ratio (*w/c*) of 0.45. Ratios of components used for the concrete are displayed in Table 3-1. Due to low workability, water reducer was added at a maximum of 1% of the cement weight. One concrete test cylinder specimen was prepared from each batch of concrete.

Table 3-1 Concrete Mix Design

Concrete Mix Design			
Material	Weight (lb)/y^3	Weight (lb)/ft^3	Weight (lb)/6 ft^3
Cement	611	22.6	135.8
Sand	1450	53.7	322.2
Stone	1600	59.3	355.6
Water	275.276	10.2	61.2

Concrete was compacted in 2" lifts. A #4 steel rebar was used to compact the concrete as it was poured to eliminate any voids especially at the bottom of the rebar cage in the tight spaces. A rubber mallet was tapped along the sides until it was evident that air bubbles were no longer floating to the top of the surface. Concrete was poured until it was flush with the forms as shown in Figure 3-4. At this point the beams were placed inside the laboratory and allowed to cure for 24 hours. Water was poured on the beams and then covered with burlap to retain the moisture as shown in Figure 3-5. This process was continued consistently for two weeks. Three days into the curing process the forms were removed. Before testing the specimens, a white latex paint was added to the bottom section of each beam. The purpose of this paint is to aid in the observation of crack development during the beam flexural test.

Figure 3-4 Concrete Beams

Figure 3-5 Curing of Concrete Beams with a Burlap Cover

3.2   Flexural Test Setup

A three-point flexural test was selected for this experiment to observe the flexural behavior. The beam was supported 1.5 in. from each edge of the beam with a clear span of 30 in. between supports. The concentrated load was applied at the midspan. Between each support and the applied load was a 15 in. spacing. The details of the testing orientation are shown in Figure 3-6.

3.3   Testing Equipment

The load was applied at the midspan of the beam with a CM-3000-SD Concrete Compression Machine. Both protective doors were opened and two shallow steel beams were placed on the base to provide a stable surface to place the beam supports at the required 30" span. A dial gauge capable of reading results to the $1/10,000^{th}$ in. and an ELE model 27-1115/02 LVDT were used to record the deflection of the beam. The setup for the experiment is shown in Figure 3-7.
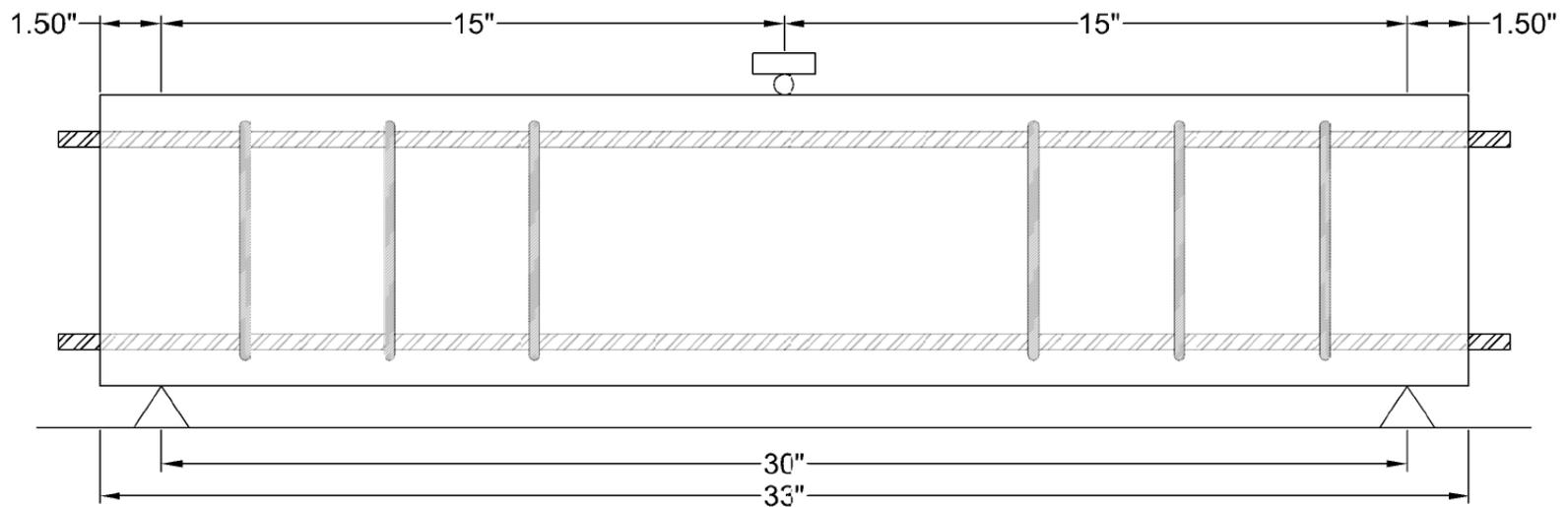
Figure 3-6 Three Point Flexural Bend Test Orientation

Figure 3-7 Final Testing Orientation

3.4 Concrete Compressive Strength

The concrete test cylinders were placed in a Gilson 200K Compression Testing Machine with a top and bottom bearing block. The cylinders were tested for compressive strength with a loading rate of 35 psi/sec ± 7 psi. as per ASTM C39 "Compressive Strength of Cylindrical Concrete Specimens". This is equivalent to an approximate range of 350 lbs. to 525 lbs. per second based on the cross section of the four inch diameter cylinders. The results of the compressive strengths are shown in Table 3-2. The modulus of elasticity (E_c) was calculated from Equation 10. The modulus of rupture was derived from Equation 7. A summary of all the characteristics of the concrete are shown in Table 3-3.

Equation 10 Modulus of Elasticity for Concrete

$$E_c = 57,000 * \sqrt{f_c'}$$

Table 3-2 Results of Concrete Compressive Tests

Concrete Cylinder Tests		
Test	Load (kips)	Compressive Strength (psi)
1	67	5332
2	64	5093
3	66	5252
Average	66	5226

Table 3-3 Concrete Data to Use for Analysis

Concrete Characteristics	
f_c' (psi)	5225
E_c (psi)	4120000
f_r (psi)	542

3.5   Beam Properties and Predicted Capacities

Based on the experimental concrete strength Figure 3-4 shows a summary of the beam properties. Table 3-5 shows the first crack moment and the nominal flexural strength for the beam; including the stress in the BFRP reinforcement and the neutral axis depth at failure based on a third-point bending test.

Table 3-4 Summary of Beam Properties and Failure Criteria

f'_c (psi)	f_y (psi)	E_c (ksi)	E_f (ksi)	ρ_f/ρ_{fb}	n	k
5225	123000	4120	6700	2.29	1.626259	0.159459

Table 3-5 Cracking Loads, Ultimate Loads, Stresses at Ultimate Load

M_{cr} (kip-ft)	M_n (kip-ft)	P_{cr} (kips)	Pn (kips)	f_f (psi)	a (in)
1.48	7.84	2.36	12.55	78153.72	0.97

4 EXPERIMENTAL RESULTS

4.1 Deflection

Due to lack of accessibility near the midspan, the dial gauge and LVDT were placed at ~10 in. from the support. Loads were applied at intervals ranging from 0.5 kips to 1.0 kips. Readings were recorded at each interval and visual observations were made regarding crack formation. Readings of the dial gauge and LVDT are shown for each of the two specimens shown in Table 4-1 and Table 4-2.At the beginning of loading on both specimens there were difficulties obtaining reliable data up to approximately 4.0 kips. After this loading point, the dial gage readings were consistent with the LVDT readings. Since there was a strong correlation between data provided by both pieces of equipment the values were averaged to represent the data for each specimen and are shown in Figure 4-1. Note that these deflections correspond to the location 10 in. from the support and not the midspan.

Table 4-1 Experimental Deflection from Dial Gauge and LVDT for Specimen 1

(Highlighted fields are assumed)

Specimen 1		
Load (lbs.)	Dial Gauge (in.)	LVDT (in.)
550	0.001	0.001
1050	0.001	0.001
1500	0.002	0.002
2000	0.002	0.002
2500	0.003	0.003
3000	0.003	0.003
3500	0.004	0.005
4000	0.006	0.007
4500	0.011	0.012
5000	0.013	0.014
5500	0.016	0.016
6000	0.020	0.020
6600	0.028	0.028
7000	0.031	0.030
8000	0.040	0.039
9000	0.052	0.051
10000	0.072	0.070
11000	0.108	0.106

Table 4-2 Experimental Deflection from Dial Gauge and LVDT for Specimen 2

(Highlighted fields are assumed)

Specimen 2		
Load (lbs.)	Dial Gauge (in.)	LVDT (in.)
1000	0.001	0.001
2000	0.002	0.002
3000	0.003	0.003
4000	0.005	0.007
5000	0.009	0.010
6000	0.017	0.019
7000	0.025	0.028
8000	0.041	0.045
9000	0.056	0.054
9700	0.070	0.072
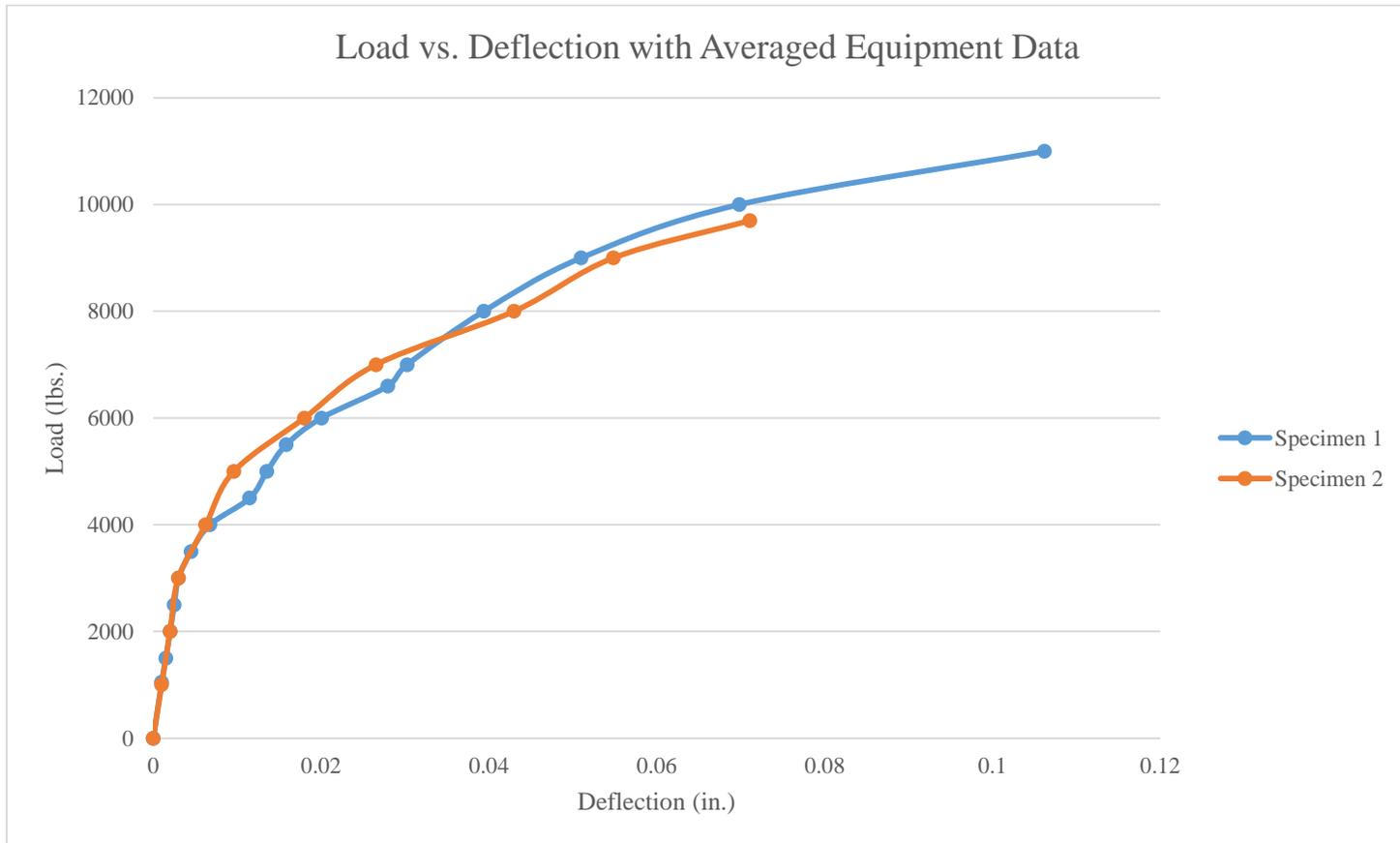
Figure 4-1 Load vs. Deflection Curves of Both Specimens

4.2 Crack Development

Due to the confined experimental setup, accessibility to beam midspan was limited for inspecting crack initiation and development. The first visual crack initiated at approximately 5500 lbs. This crack extended approximately half way up the cross-section as shown in Figure 4-2. It seems that the first crack initiated before this based on the load deflection curve. Cracking started with a pronounced flexural crack followed by a shear flexure crack developing on each side of the first crack (Figure 4-3). The cracks continued to propagate to the top of the beam. At final failure, the concrete crushed which is reflective of an over-reinforced beam. Only a few very pronounced cracks were observed and this pattern was similar to research finding reported by Urbanski, Lapko and Suprynowicz (2015). This indicates a strong bond between the rebar and concrete. Unfortunately, crack width data could not be measured during the experiment.

Figure 4-2 First Crack in Specimen 1

Figure 4-3 Shear Flexure Cracking

4.3   Failure

For Specimen 1 there was an ultimate load of approximately 11000 lbs. before failure.

Specimen 2 failed at 9700 lbs. Specimen 1 had consistent cracking on both sides of the

beam, whereas Specimen 2 had significant cracking on one side of the beam and little to

no cracking on the other side until close to failure. The crack behavior was very similar in

both beams which was expected due to the lack of shear reinforcement located in the

middle third of the beam. Overall, the results indicate the specimens were stiffer than

expected. This could be due to the short span length that negated the effects of cracking on

the curvature of the beam. A more precise method of acquiring deflection data would be

ideal for future research.

5   NUMERICAL MODELING OF BFRP REINFORCED CONCRETE BEAM

USING ANSYS

5.1   Background

The BFRP reinforced concrete beams were modeled using ANSYS Mechanical APDL. Using this module, a nonlinear analysis was performed that considered crack initiation and growth in the beam and the nonlinear behavior of concrete. This numerical model allows deflection computation at any load step and comparison with the experimental and results. Additionally, stresses and strains can be determined at any applied load after the first crack.

5.2   Elements and Materials

Concrete is a quasi-brittle material that exhibits different behavior in compression and tension. ANSYS provides an element known as a SOLID65 that can be used to model concrete. This solid can crack in tension and crush in compression. The element consists of 8 nodes having three degrees of freedom at each node as shown in Figure 5-1 (ANSYS ELEM)
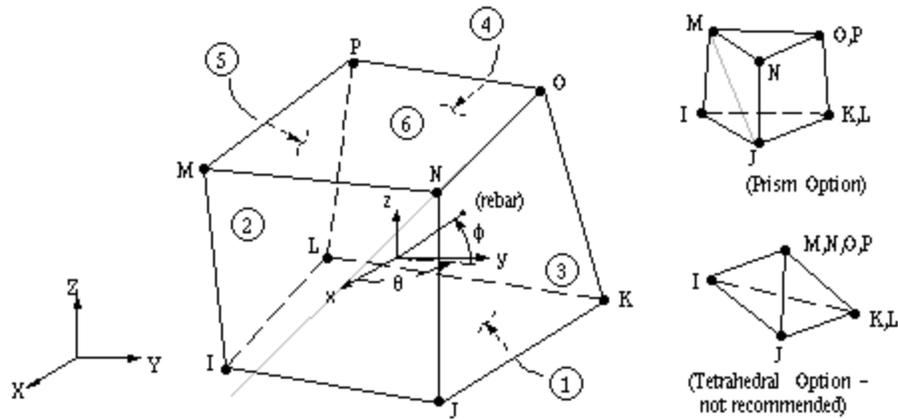
Figure 5-1 Solid65 Element (ANSYS Elem, 2015)

The concrete element will crack or crush if it is outside of the failure surface. This can be expressed as follows in Equation 11 (Willam and Warnke, 1975; cited in ANSYS Theory, 2015).

Equation 11 Failure Criterion for Concrete (ANSYS ELEM)

$$\frac{F}{f_c} - S \geq 0$$

Where:

$F = a\ function\ of\ the\ principal\ stress\ state\ (\sigma_{xp}, \sigma_{yp}, \sigma_{zp})$

$S = failure\ surface\ based\ on\ principal\ stresses\ and\ f_t, f_c, f_{cb}, f_1, f_2$

$f_c = uniaxial\ crushing\ strength$

$$\sigma_{xp}, \sigma_{yp}, \sigma_{zp} = principal\ stresses$$

TBDATA inputs are necessary to reflect the above criterion. The TBDATA required is shown in Table 5-1 from ANSYS E Element Reference Manual. This table lists all the required constants. Table 5-2 further explains these constants in terms of material properties. If constants 1-4 are input, then 5-8 will default to the values shown in Table 5-1. Shear transfer coefficients range from 0 to 1 with 0 representing a smooth crack and 1

representing a rough crack without any loss of shear transfer (ANSYS Elem, 2015).

Various studies recommend values for the open crack shear transfer coefficient to range

from 0.2 to 0.5 (Bangash, 1989; Hemmaty, 1998; Huyse, Hemmaty and L.Vandewalle,

1994). Uniaxial tensile cracking stress comes from Equation 7. Uniaxial crushing stress is

derived from the concrete cylinder tests in Table 3-2.

Table 5-1 Real Constant Data Required for SOLID65 Element (ANSYS Elem, 2015)

TBDATA Concrete	
Constant	Meaning
1	Shear transfer coefficients for an open crack.
2	Shear transfer coefficients for a closed crack.
3	Uniaxial tensile cracking stress.
4	Uniaxial crushing stress (positive).
5	Biaxial crushing stress (positive).
6	Ambient hydrostatic stress state for use with constants 7 and 8.
7	Biaxial crushing stress (positive) under the ambient hydrostatic stress state (constant 6).
8	Uniaxial crushing stress (positive) under the ambient hydrostatic stress state (constant 6).
9	Stiffness multiplier for cracked tensile condition, used if KEYOPT(7)=1 (defaults to 0.6).

Table 5-2 Material Properties for Each Constant (ANSYS Theory, 2015)

	Reference for TBDATA	Constant
f_t	Ultimate uniaxial tensile strength	3
f_c	Ultimate uniaxial compressive strength	4
f_{cb}	Ultimate biaxial compressive strengt	5
σ^a_h	Ambient hydrostatic stress state	6
f_1	Ultimate compressive strength for a state of biaxial compression superimposed on hydrostatic stress state σ^a_h	7
f_2	Ultimate compressive strength for a state of uniaxial compression superimposed on hydrostatic stress state σ^a_h	8

Rebar modeling in concrete can be accomplished with the LINK180 element. This is

a spar element with three degrees of freedom at each node (ANSYS Elem, 2015). These

elements are capable of handling nonlinear behavior which can be modeled relatively well

with a bilinear isotropic definition. Although the BFRP rebar does not yield, bilinear behavior was utilized.

Incorporating the rebar into the model can be done with three different model types; discrete, embedded and smeared as shown in Figure 5-2. The discrete model attaches the beam elements to the concrete mesh nodes and is limited to the meshing of the concrete. It is important to note that the volume is not deducted from the concrete. The embedded model is commonly modeled with the reinforcing stiffness separate than the concrete stiffness and is not limited to the meshing of the concrete. This increases the number of nodes and DOF and may increase processing time. The smeared model uniformly spreads the reinforcement throughout the concrete elements in a defined section (Wolanski, 2004).

The impactor (bearing plate) and supports were modeled using a SOLID185 element. This is similar to the SOLID65 element with eight nodes and three degrees of freedom. This element was used specifically to distribute the load to `prevent stress concentrations that would affect the convergence. In order to accomplish this rigid surface a high modulus of elasticity was input matching that of steel.
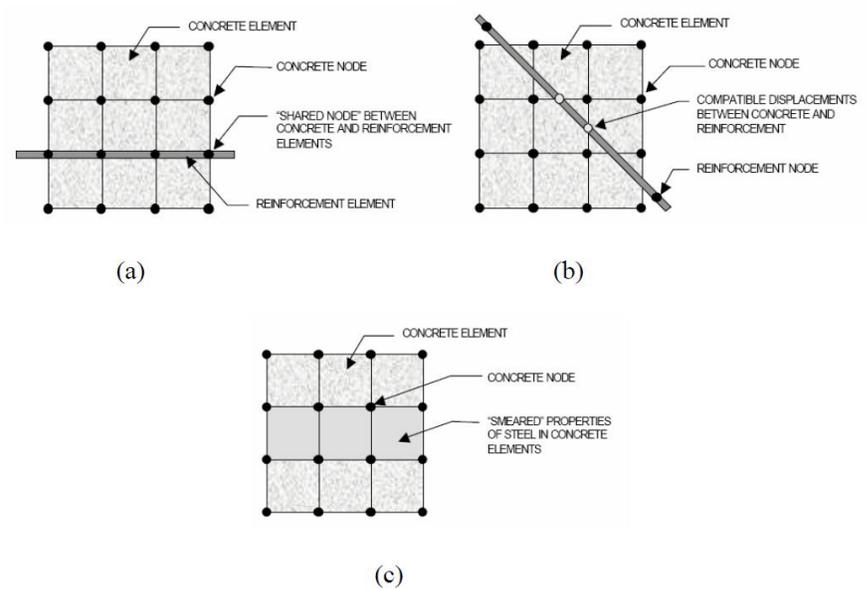
Figure 5-2 Types of Reinforcement Modeling (a) Discrete, (b) embedded, (c) smeared

(Tavarez, 2001)

A summary of all the inputs used for solid elements and link elements are shown in Table 5-3 and Table 5-4 respectively. As previously mentioned bilinear behavior was input for the BFRP rebar in case there were convergence issues near failure. The BFRP stirrup hanger was incorporated into the model to investigate the effects on overall stiffness. According to Prachasaree, Piriyakootorn, Sangsrijun & Limkatanyu (2015), the compressive capacity of FRP reinforcement may range from 30-50% of the ultimate tensile strength. For purposes of this research a conservative value of 30% was input.

Table 5-3 Input Data for Solid Elements

Component	Material	Element Type	Material Properties		
Concrete	1	SOLID65	Linear Isotropic		
			EX (psi)	4125000	
			NUXY	0.3	
			Multilinear Isotropic		
			Point	Strain	Stress
			1	0.00000	0.0
			2	0.00038	1567.5
			3	0.00075	2841.5
			4	0.00100	3565.7
			5	0.00150	4578.7
			6	0.00200	5080.9
			7	0.00254	5225.0
			8	0.00300	5225.0
			9	0.00350	5225.0
			Concrete (Per Table XX)		
			Constant	Value	
			1	0.3	
			2	0.8	
			3	542.1	
			4	-1	
			5	0	
			6	0	
			7	0	
			8	0	
			9	0	
Impactor	4	SOLID185	Linear Isotropic		
			EX (psi)	29000000	
			NUXY	0.3	

Table 5-4 Input Data for Link Elements

Component	Material	Element Type	Material Properties		
BFRP Rebar (TENSION)	2	LINK180	Linear Isotropic		
			EX (psi)	6700000	
			NUXY	0.3	
			Bilinear Isotropic		
			Yield (psi)	123000	
			Tang Mod	6700	
			Cross-Section		
			A (in2)	0.1104466	
Steel Stirrups	3		Linear Isotropic		
			EX (psi)	29000000	
			NUXY	0.3	
			Bilinear Isotropic		
			Yield (psi)	45,000	
			Tang Mod	29000	
			Cross-Section		
			A (in2)	0.0490874	
BFRP Rebar (COMPRESSION)	5		Linear Isotropic		
			EX (psi)	6700000	
			NUXY	0.3	
			Bilinear Isotropic		
			Yield (psi)	123000	
			Tang Mod	6700	
			Cross-Section		
			A (in2)	0.1104466	

5.3   Constructing Numerical Model

5.3.1   Command File

To create the model a command file was created due to difficulties of navigating the graphical user interface (GUI) of ANSYS Mechanical APDL. Input files are capable of running and processing an entire project, but this command ended at the solution section which requires the user to input some final information for solution commands such as convergence tolerance and load steps. The full command file is located within Appendix.

5.3.2   Creating Solids

The first step to create a solid key points is defined in the command file that reflected the eight corners of the shapes. Once these points are defined a volume can be created as shown in Figure 5-3. At this point the respective concrete element and material type were selected and the volume was meshed with 1 in. element sizes. All items were selected and the component was created. The same process was repeated for the impactor and supports. Figure 5-4 displays the model at this point.

5.3.3   Creating Lines

Line elements were also created using key points. After the line is created the element and material type were selected for the respective lines. The element size was defined as 1 in. and then meshed. This is similar to the solids in order for the nodes to coincide for simplicity. Components were created for the BFRP rebar, BFRP hanger and steel stirrups. Figure 5-5 shows all the line elements.

5.3.4   Boundary Conditions, Contact Surfaces and Applied Loads

The model requires satisfactory boundary conditions in order to solve the problem. Firstly, the supports and impactor were connected to the concrete surface using the

45

CEINTF command. This contact surface was assigned a tolerance interval of 0.01. To connect the reinforcement to the concrete elements **NUMMRG** command was applied to all the LINK180 and SOLID65 elements. This command merges all coincident nodes.

The experiment could be modeled as a simply supported beam because no rotation was restricted at either end and displacement along the length of the beam is allowed since the supports are not fixed to the beam. A typical simple support consists of a pinned condition on one end a roller condition on the other. In finite element analysis, it is common to have the y-axis oriented vertically, the x-axis to be along the beam and the z-axis to be transverse to the length of the beam. Therefore, in terms of the coordinate system of the model that is the equivalent to setting the displacement in the x, y and z directions to zero at one end and setting the displacement in the y and z direction to zero on the other end. This allows the beam to translate along the length similar to a roller. If this end was fixed in three directions, there would be artificial fixity that does not exist in reality. These DOF constraints are applied at the nodes along the center of the supports.

The ultimate failure load from the experiment and analysis indicated that 10 kips applied at the midspan would cause complete failure or partial collapse of the structure. To load the impactor with 10 kips the value was divided by the number of nodes along the z-axis of the support. The equivalent nodal force to be applied was 2 kips per node. Figure 5-6 shows the constraints and loads applied to the model.
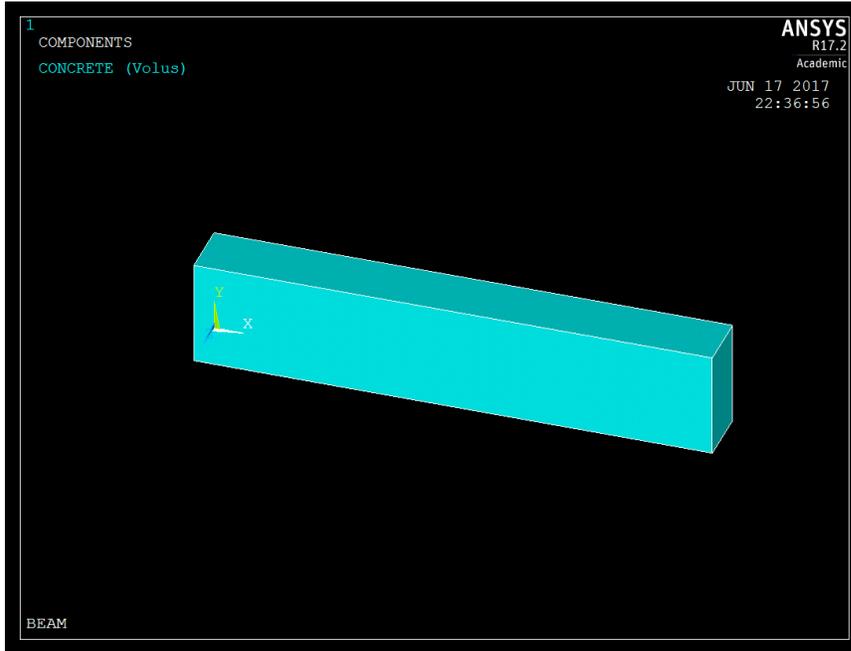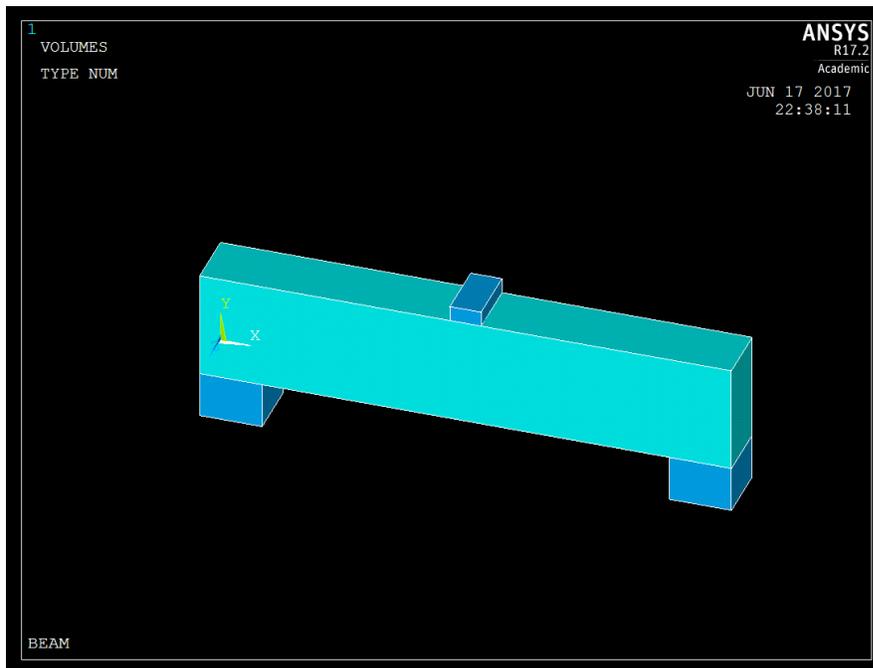
Figure 5-3 Concrete Volume
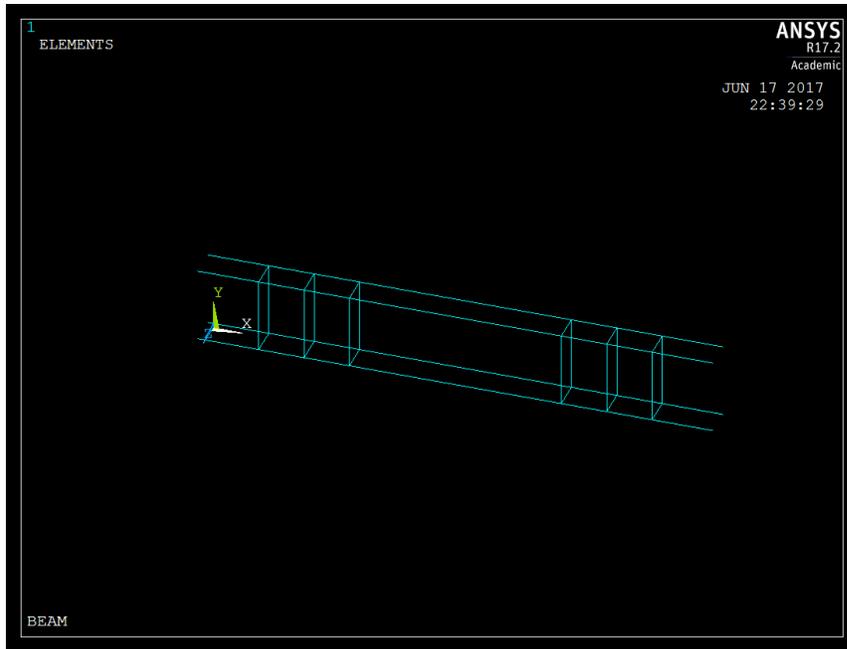

Figure 5-4 All Volumes

47

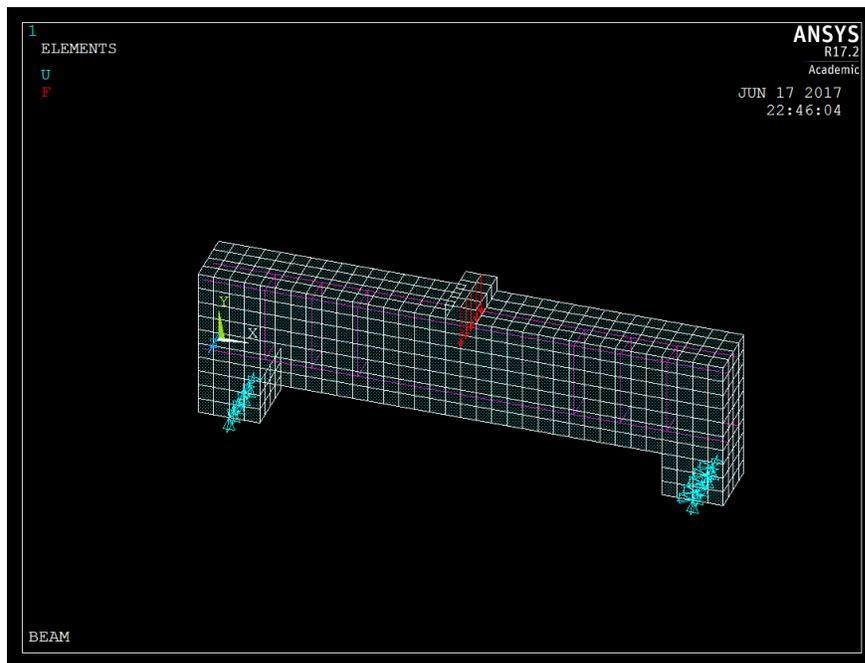*Figure 5-5 All Line Elements for Reinforcement*

Figure 5-6 Final Model Showing DOF Constraints and Applied Loads

5.3.5   Solution Controls

SOLID65 elements are notorious for having convergence issues due to the cracking and crushing of the elements. This required customization of the solution parameters in order to converge on an accurate solution. The parameters were set to follow the research conducted by Wolanski, 2004. In this research Wolanski was able to replicate a previous experiment accurately with his model. The first step of the solution input was to set the analysis type to structural. Then in the Basic section the time at end of load step was set to 1500. This means that the 10 kips will be divided into 1500 increments so very small loads are applied at each step up to the final load. At each increment this allows better convergence using the previous iteration as a reference. The number of substeps, max. number of substeps and min. number of substeps were all set to 1500. In the Sol'n Options tab everything was left as default except the Sparse Direct equation solver was selected. In the nonlinear tab the Line search option was turned off and max number of iterations was set to 150. Convergence criteria was set as follows: F, 0.005 and U, 0.05. Default values were kept in the Advanced NL tab except the program behavior upon no convergence was set to 'Terminate but Do Not Exit'.

5.4   Solution

The model successfully completed all 1500 time steps indicating the beam did not reach complete failure. It was determined that the first crack occurred at 2935 lbs. at which point processing in the nonlinear region slowed the convergence of each time step. Once the solution was completed the results were read from various load steps to verify that the model was behaving as expected. Images were captured from ANSYS at loads of 2000,

2933, 2967, 7500 and 10000 lbs. which reflects the linear elastic region, the time just before of first crack, just after first crack, the nonlinear region and the final load respectively.

Figure 5-7 - Figure 5-10 shows the y-axis deflection contour plot at each of the load steps. There is a clear increase in deflection as load is applied which indicates the model is behaving properly. The supports also show that rotation was not constrained and the deflected shape is correct.
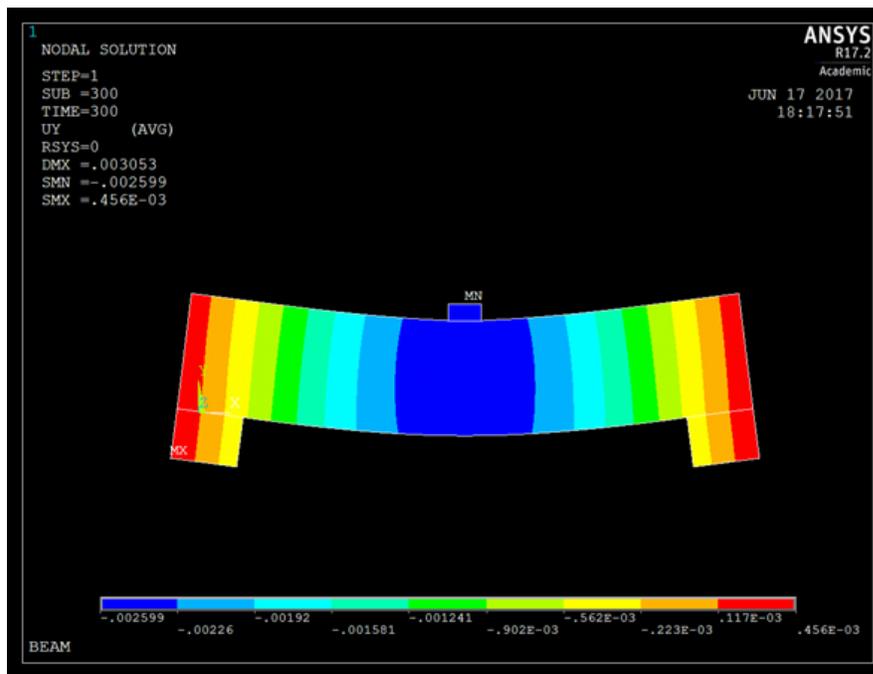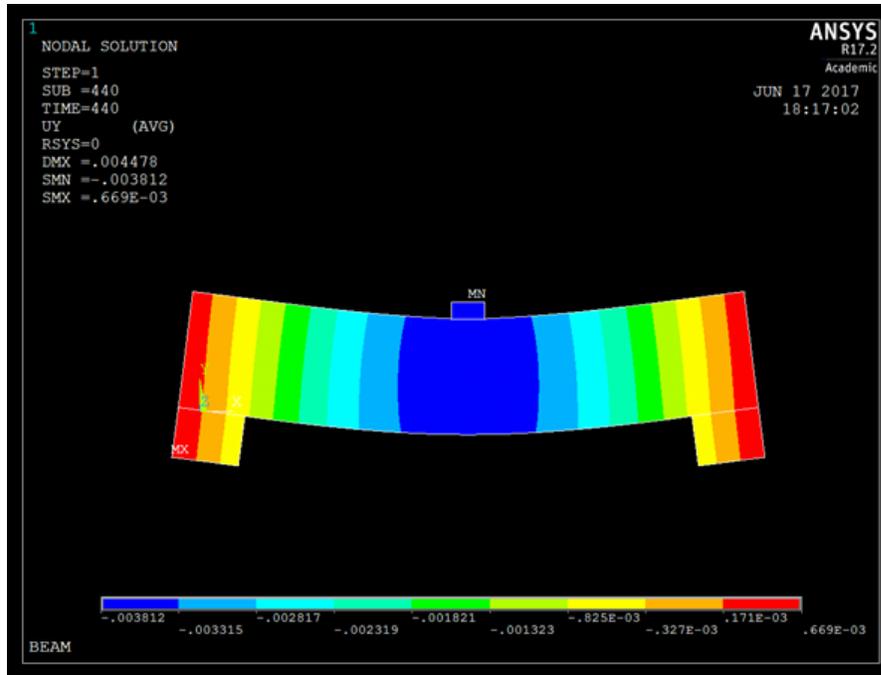

Figure 5-7 Y-Deflection at 2000 lbs.
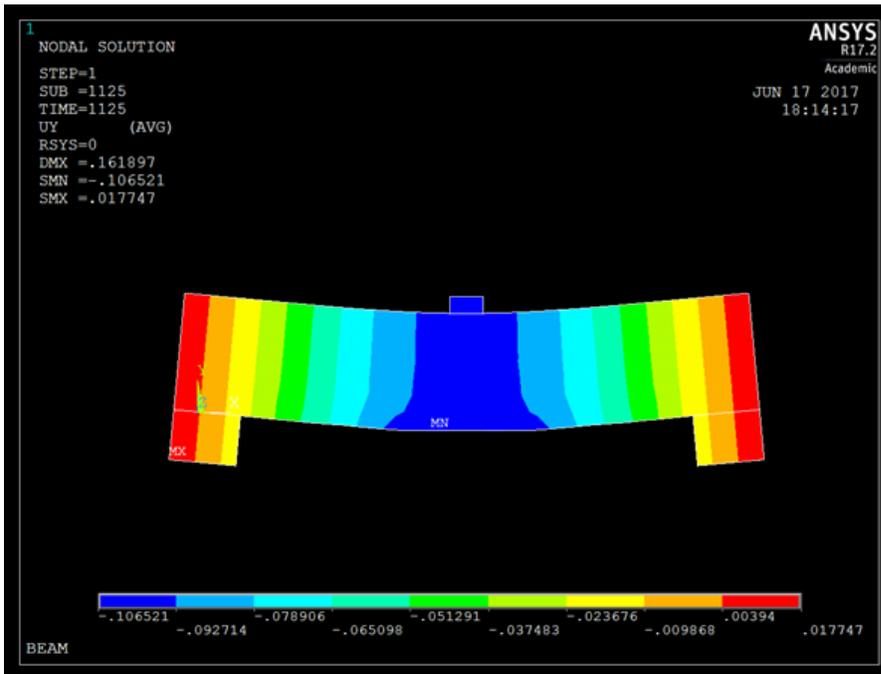
Figure 5-8 Y-Deflection at 2933 lbs.

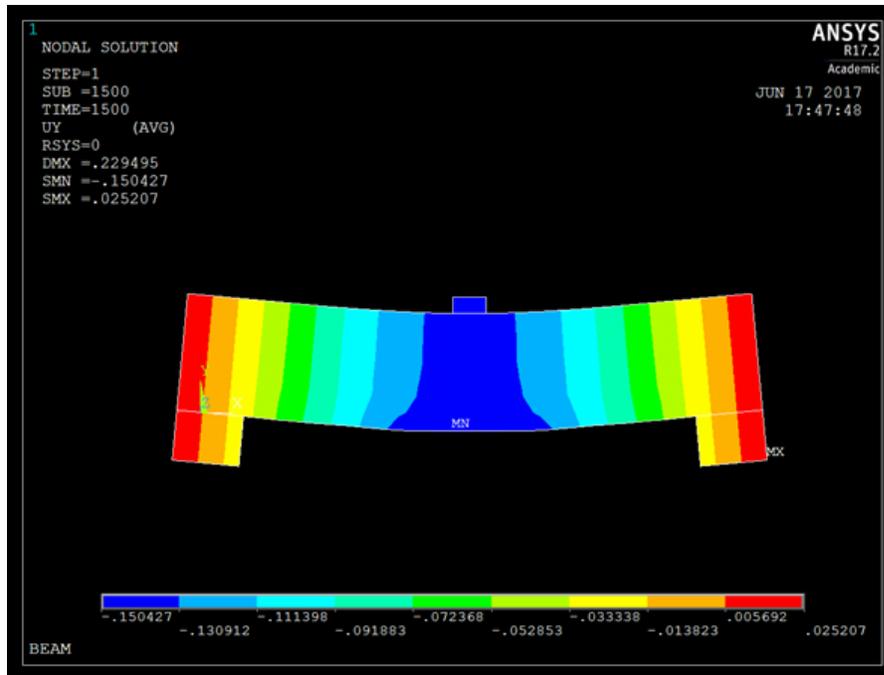*Figure 5-9 Y-Deflection at 7500 lbs.*

51

Figure 5-10 Y-Deflection at 10000 lbs.

The elastic stress along the x-axis is shown in Figure 5-11-Figure 5-14. This reflects the internal compression and tension of the beam to resist the applied moment. Just before the first crack it is shown that the concrete in the tension zone reaches a stress of 573 psi which is slightly larger than the tensile strength of 542 psi as calculated. As the load increases the over-reinforced behavior becomes more evident as the concrete approaches its compressive strength shown by the bluish contours on the top of the beam. Figure 5-15-Figure 5-18 shows the elastic stresses for the reinforcement. There is a clear increase in stress up to the cracking load. Nonlinearity is evident by the high stresses at the 7500 and 10000 lbs. load. The beam was very over-reinforced so the rebar reaches approximately half of its ultimate tensile strength of 123 ksi. The shear reinforcement was highly effective after cracking which is shown by the lighter shades of blue. This is a tensile reaction in the reinforcement to resist the principal stresses associated by the shear at the supports. It is interesting to note in Figure 5-17 that the maximum principal stress at the support are at

52

approximately 45 degrees denoted by the lighter blue contour in the shear stirrups. The compression rebar was also engaged shown by the dark blue contour indicating the highest compression in the reinforcement system. The lighter contours may be from cracking or stress concentrations at the location of the impactor.
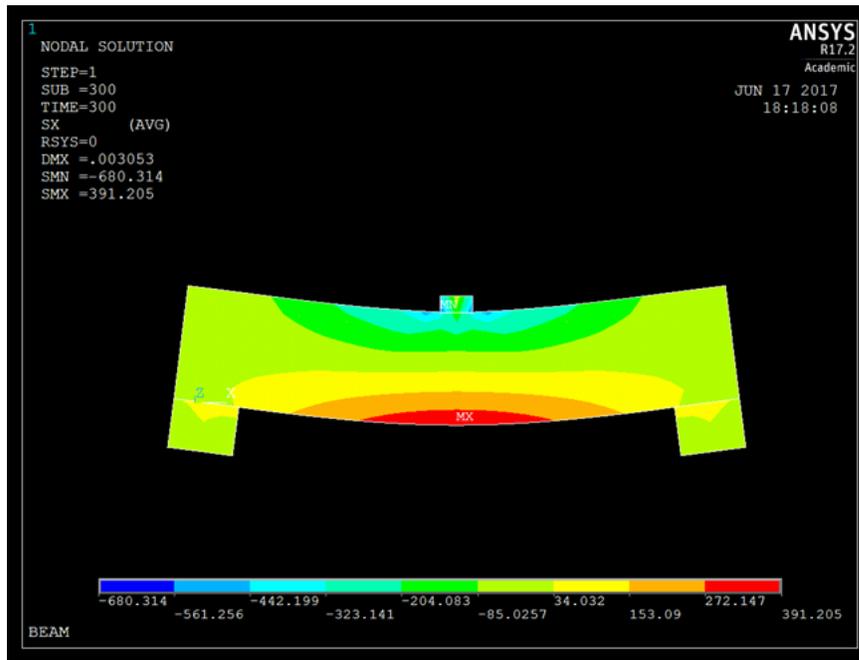

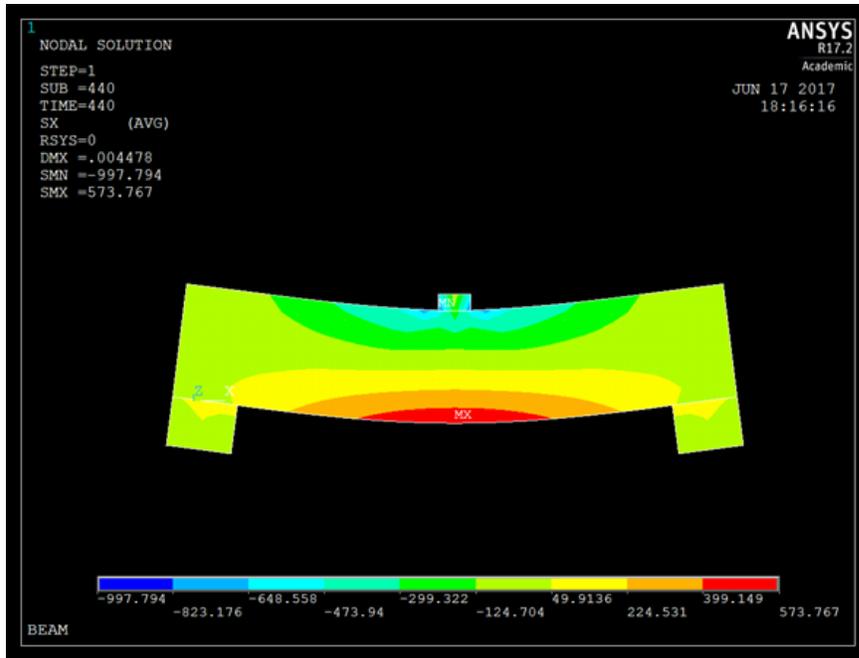*Figure 5-11 X-Direction Stresses at 2000 lbs.*

`

Figure 5-12 X-Direction Stresses at 2933 lbs.
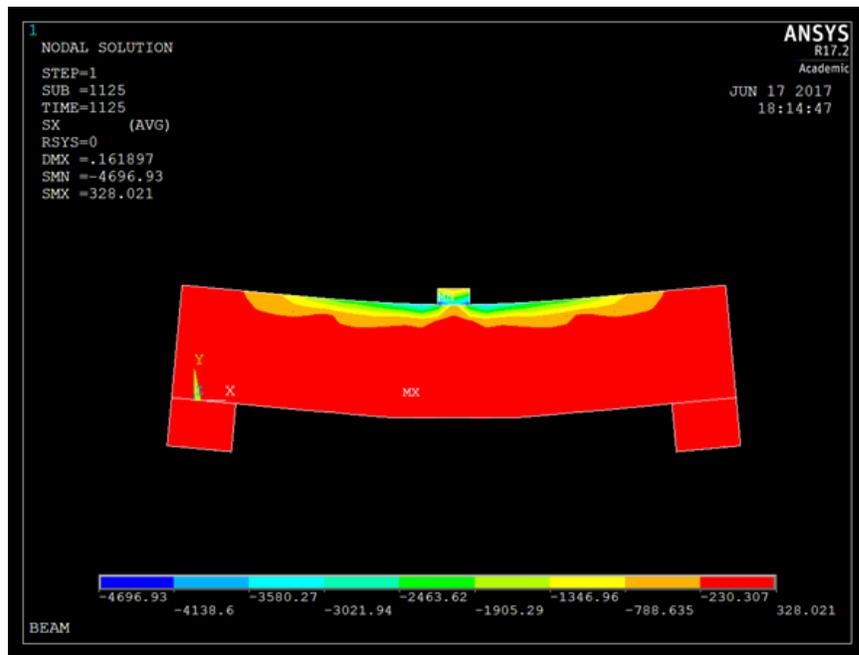
Figure 5-13 X-Direction Stresses at 7500 lbs.
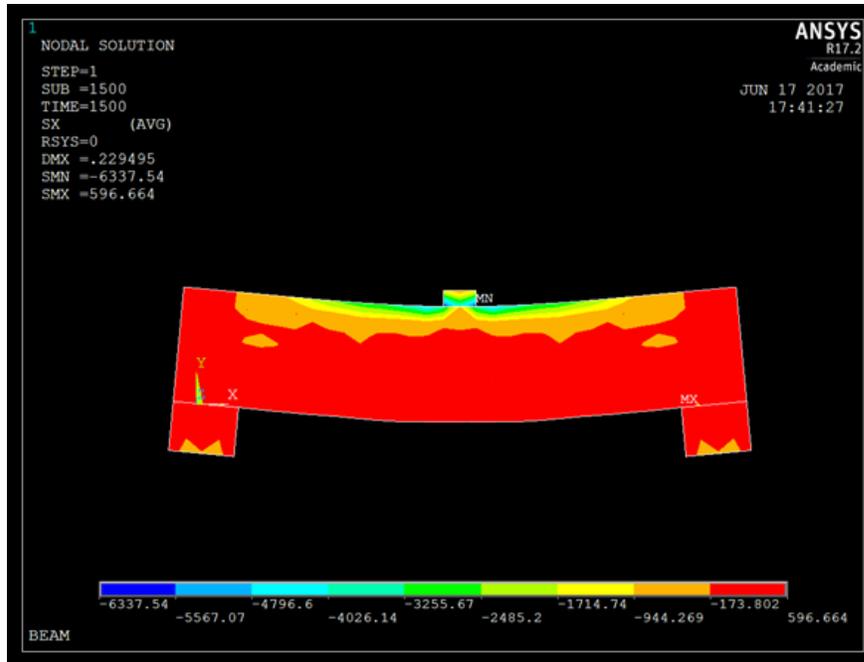
Figure 5-14 X-Direction Stresses at 10000 lbs.
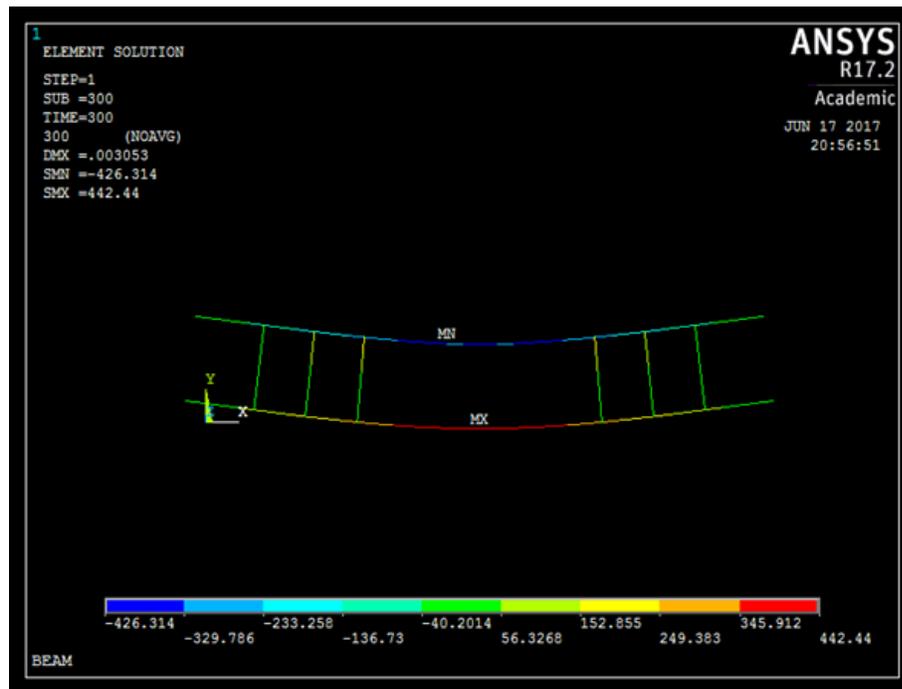
Figure 5-15 Reinforcement Stresses at 2000 lbs.

55
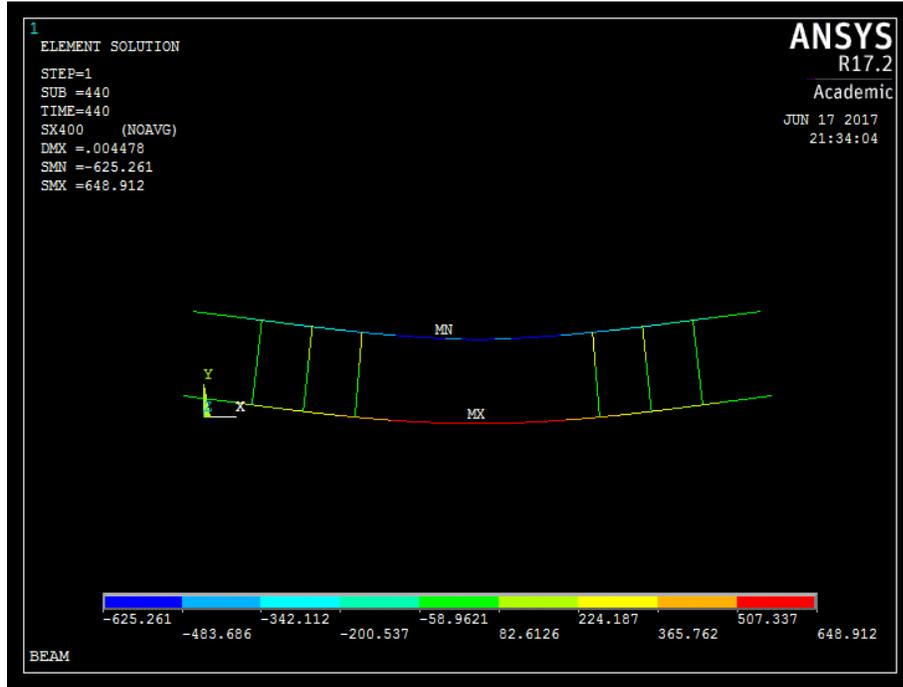
Figure 5-16 Reinforcement Stresses (psi) at 2933 lbs.
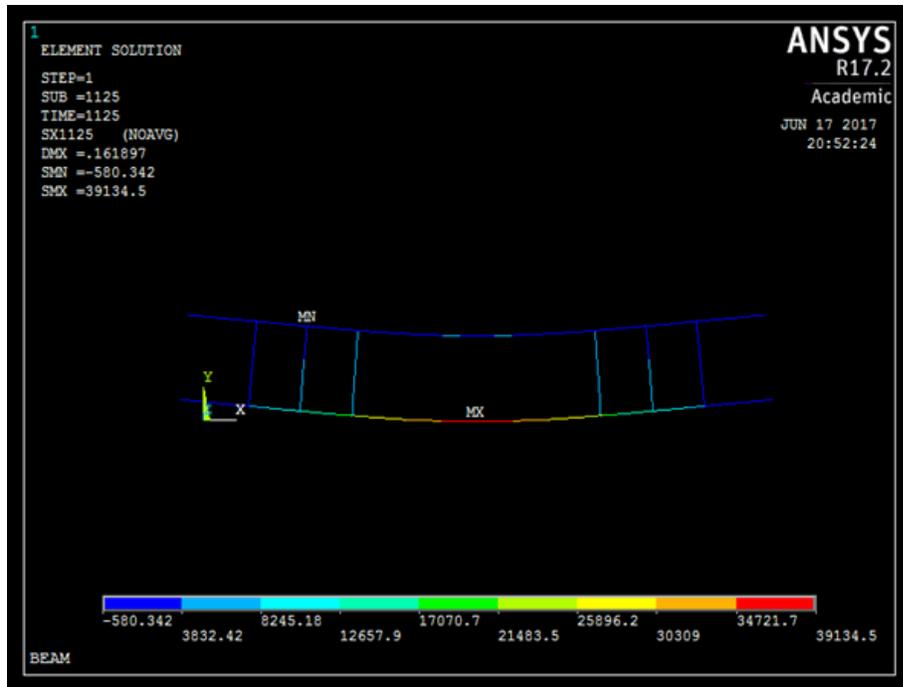
Figure 5-17 Reinforcement Stresses (psi) at 7500 lbs.
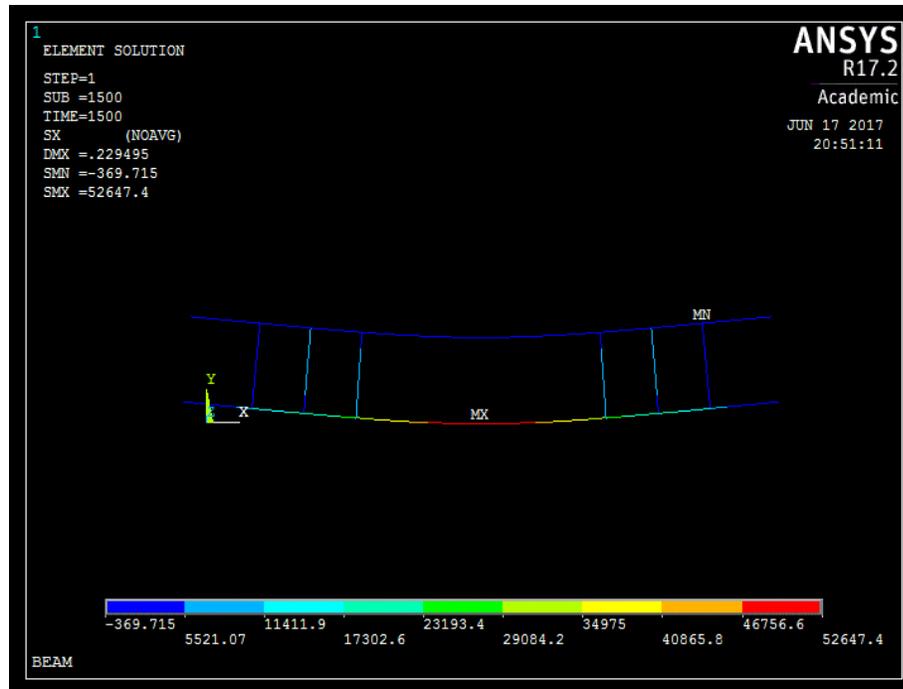
Figure 5-18 Reinforcement Stresses (psi) at 10000 lbs.

Von Mises stresses were also captured in Figure 5-19-Figure 5-22 since these are an excellent tool to gauge the overall stresses acting on a finite element. This stress will also include shear and stresses associated with the expansion and contraction of elements following Poisson's ratio. The results are similar to the x-direction stresses since there is only a uniaxial stress that is applied.

Although the SOLID65 element is capable of considering the crack/crush plot, this does not consider stress concentrations and energy methods that are typically involved with crack initiation and propagation. As a result, the face appears to be overly cracked and crushed. Up to the load of 2933 lbs. there are no recorded cracks. Immediately after cracks as shown in Figure 5-25 there is the initiation of cracks. As the load continues the cracking propagates. At the final load it appears the entire concrete cross section has been virtually cracked. The crack plots associated with each load scenario are provided in Figure 5-23-Figure 5-27.
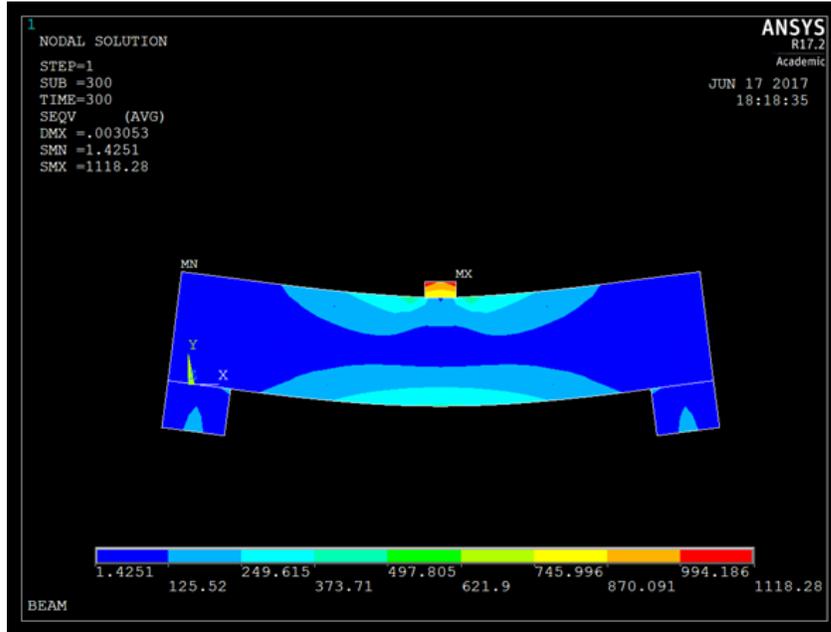
Figure 5-19 Von Mises Stress (psi) at 2000 lbs.
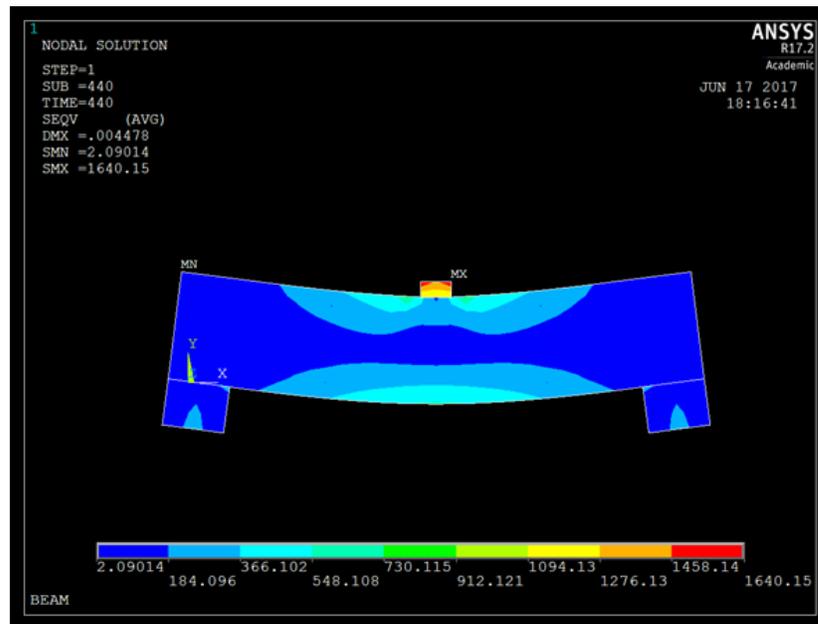
Figure 5-20 Von Mises Stress (psi) at 2933 lbs.
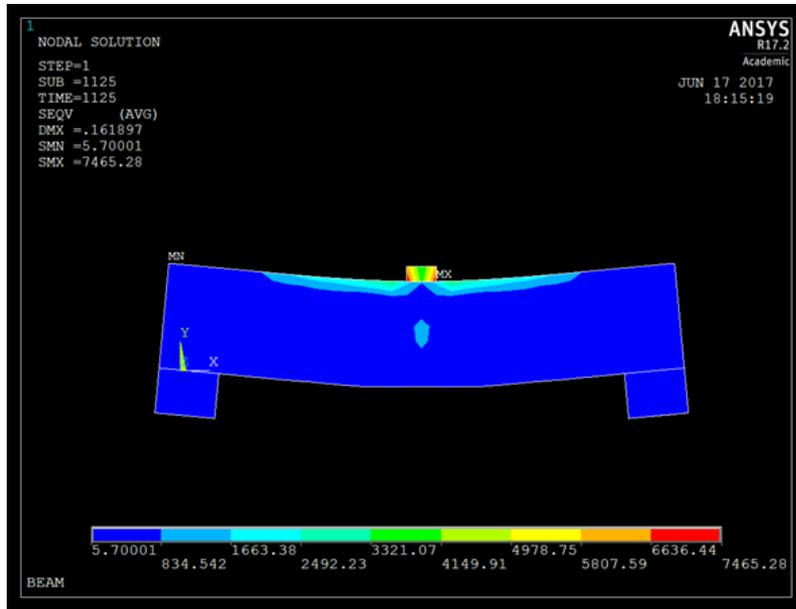
Figure 5-21 Von Mises Stress (psi) at 7500 lbs.
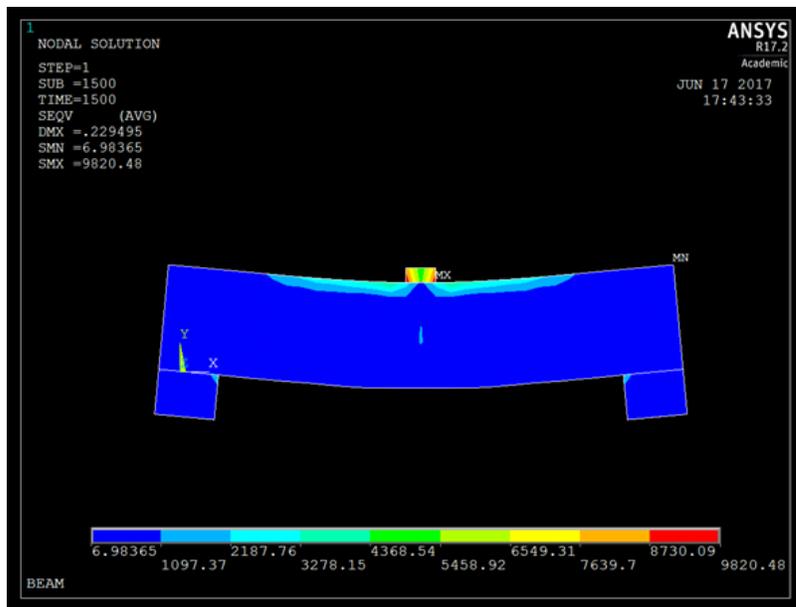
Figure 5-22 Von Mises Stress (psi) at 10000 lbs.

Figure 5-23 Concrete Crack Plot at 2000 lbs. in Linear-Elastic Range
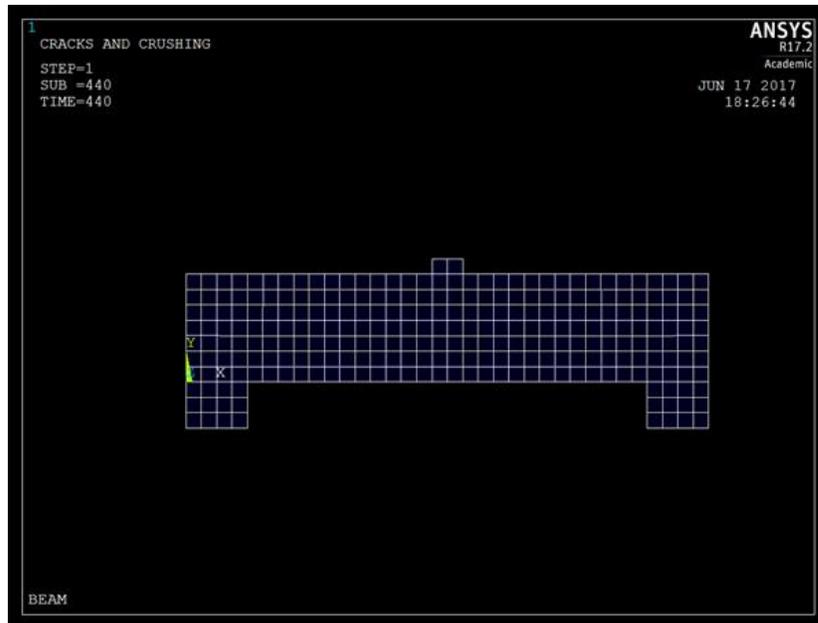
Figure 5-24 Concrete Crack Plot at 2933 lbs. Before First Crack

Figure 5-25 Concrete Crack Plot at 2967 lbs. After First Crack

Figure 5-26 Concrete Crack Plot at 7500 lbs. in Nonlinear Range
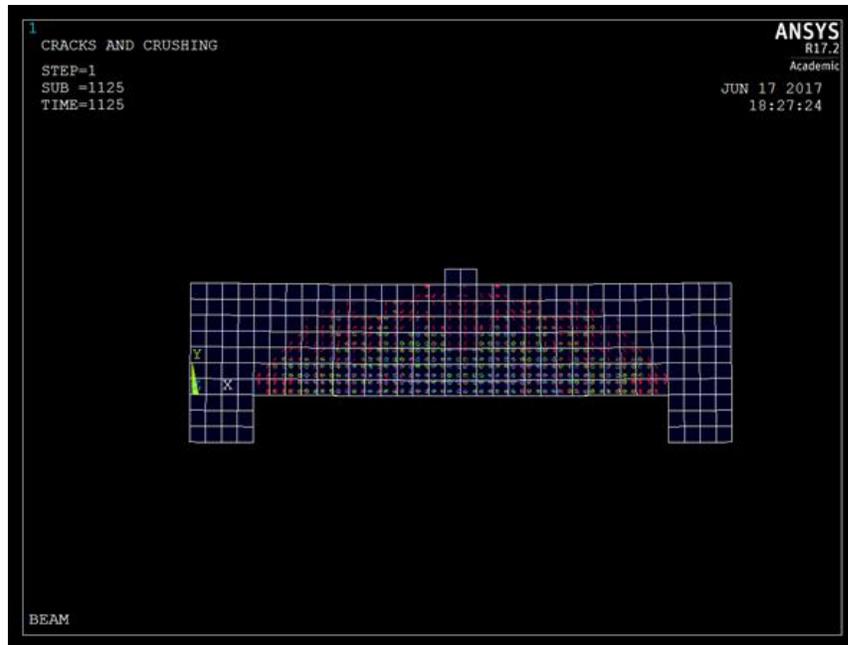
Figure 5-27 Concrete Crack Plot at 10000 lbs.

ANSYS is capable of producing time history data for nodes and elements. In order to compare deflections with the experiment an element chosen 10 in. from the center of the support was selected. Using this time history data, Figure 5-28 indicates a very stiff beam up until the cracking load. At this point the beam becomes less stiff and adheres to a less steep slope. To verify the reinforcement was behaving correctly a time history was also taken of the line stress in the element to the left of the center of the bottom and top reinforcement (Figure 5-29 and Figure 5-30 respectively). The bottom reinforcement started to take on significantly more stress after the first crack as the tension previously taken by the concrete was transferred to the BFRP. The top reinforcement shows conflicting data which may be due to stress concentrations near the impactor. Although the neutral axis of the concrete should have been less than 1 in., this is still deeper than the reinforcement and should have remained in compression over the course of the loading.

Overall, the ANSYS model performed in a manner that would indicate a properly created model. The deflection behavior matched that of the theoretical expectations. The first crack occurred almost exactly as predicted. The transfer of loads to the rebar was proven through post processor commands.
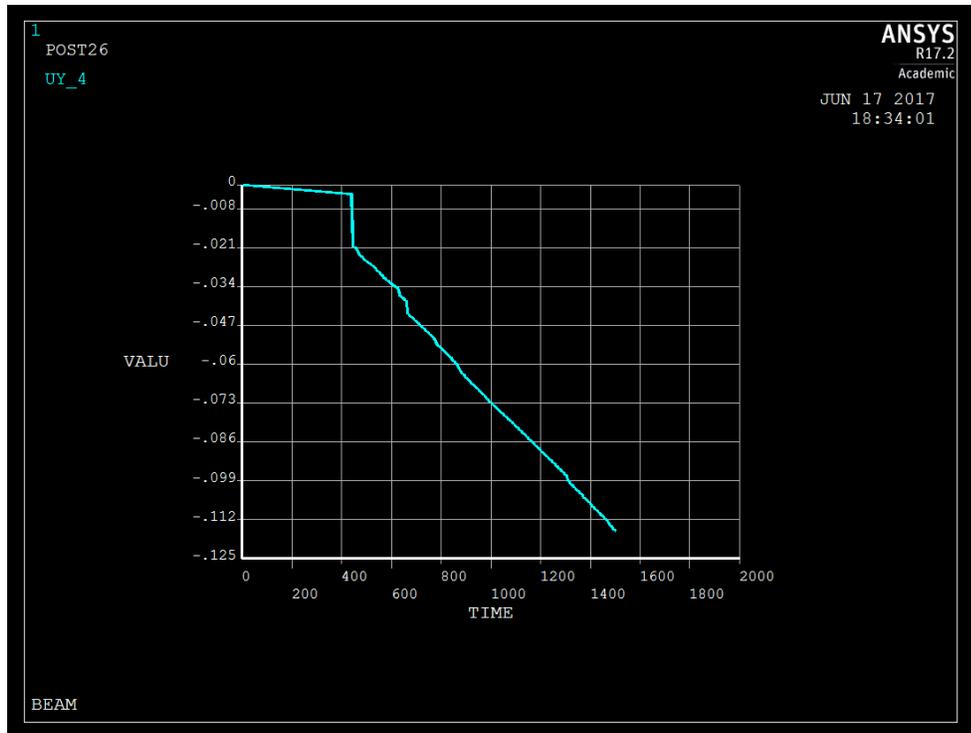
Figure 5-28 Deflection (in) vs. Time (Load) Curve at 10 in. From Support
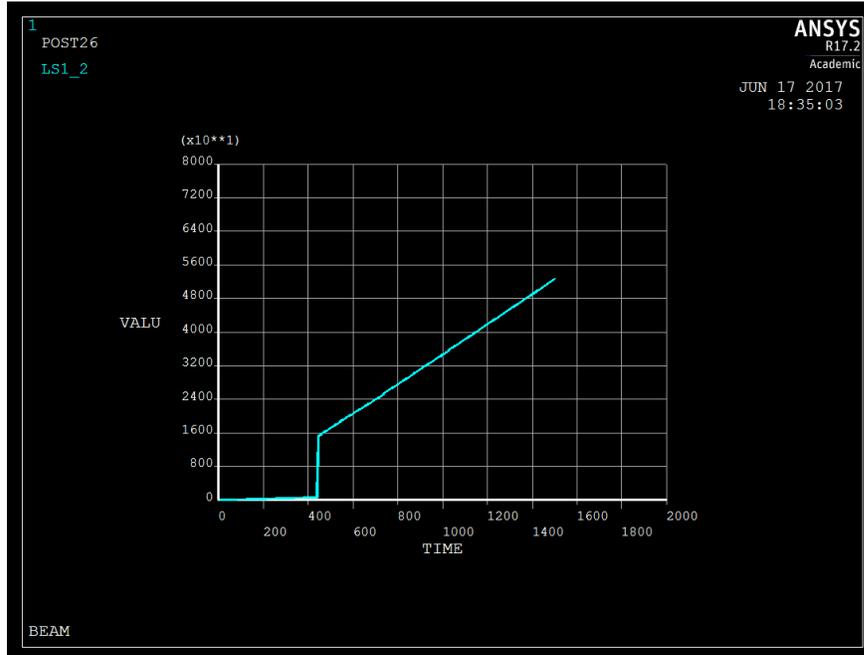
Figure 5-29 Stress (psi) vs Time (Load) of Bottom Reinforcement
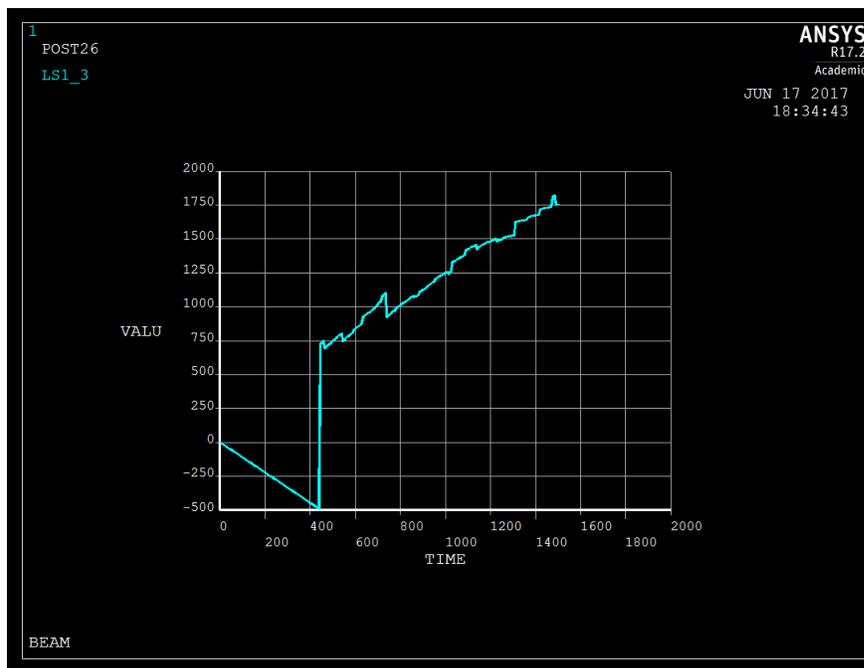
Figure 5-30 Stress (psi) vs. Time (Load) of Top Reinforcement

6   RESULTS AND DISCUSSIONS

6.1   Comparison of Analytical Results

Designing an over-reinforced BFRP beam is not typical in normal use of reinforced concrete designs. Steel yielding is sought because of the ductile failure that provides ample warning of impending collapse. To gain a better understanding of the behavior of over-reinforced beams, the results from experimental, analytical and numerical models are compared. Since crack growth pattern was not accurately recorded, the load vs. deflection will be discussed.

The three analytical models are tabulated in Table 6-1 and plotted in Figure 6-1. Branson's equation is clearly the least conservative measure for deflection which is logical because it did not consider the true behavior of FRP reinforced concrete since the derivation was from steel reinforced concrete beams. Table 6-2 compares percentage difference of predicted deflection of both ACI recommended equations, to Branson's equation. Just after reaching the cracking moment, the modified Branson equation estimates 2.14 times greater deflection than Branson's equation. The predicted deflection then begins a trend toward converging within 1.06 times Branson's equation at failure load. The ACI 440.1r-15 equation only overestimates deflection by a factor of 1.48 after the first crack and then reaches a maximum deviation of 2.10 from Branson's. This equation also begins to converge within 1.03 times Branson's equation at failure load. These are significant deviations that exist after cracking in the BFRP members. For scenarios that serviceability controls design even subtle differences can become costly and wasteful when

65

a stiffer member needs to be designed to account for such deflections. Overall, the two models from recent editions of ACI-440 which account for decreased stiffness in the members show reasonable correlation with respect to each other.

Table 6-1 Estimated Deflection Based on Analytical Models for FRP Reinforcement

Theoretical Results			
Load	Branson Deflection	Modified Branson Deflection	ACI 440-1r-15 Deflection
0	0.000	0.000	0.000
500	0.001	0.001	0.001
1000	0.001	0.001	0.001
1500	0.002	0.002	0.002
2000	0.002	0.002	0.002
2500	0.003	0.007	0.005
3000	0.006	0.012	0.012
3500	0.010	0.019	0.020
4000	0.015	0.026	0.028
4500	0.021	0.034	0.035
5000	0.028	0.042	0.043
5500	0.036	0.050	0.050
6000	0.044	0.058	0.057
6500	0.052	0.065	0.064
7000	0.060	0.072	0.071
7500	0.067	0.080	0.077
8000	0.075	0.087	0.084
8500	0.083	0.093	0.090
9000	0.090	0.100	0.097
9500	0.098	0.107	0.103
10000	0.105	0.113	0.110
10500	0.112	0.120	0.116
11000	0.119	0.126	0.122
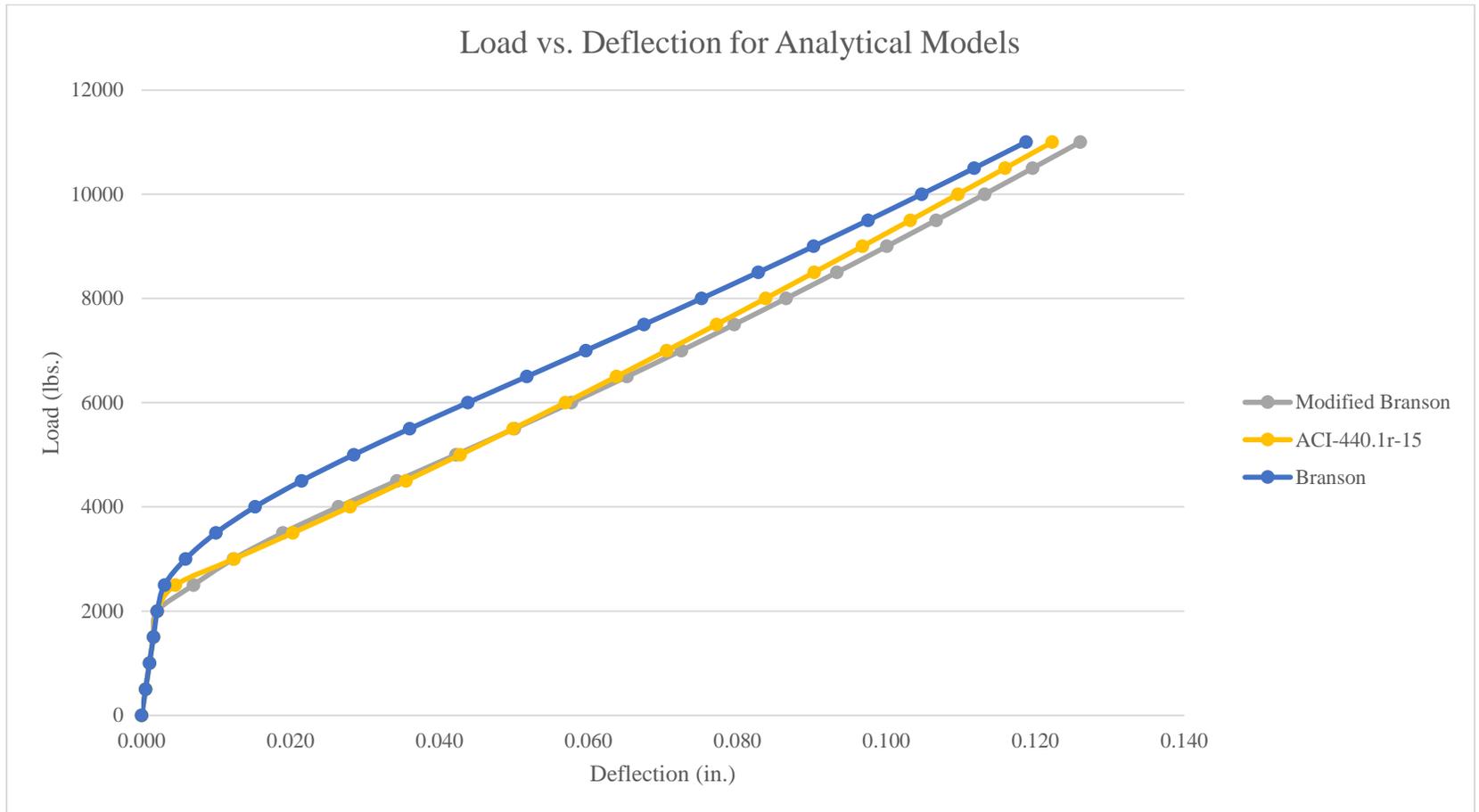
Figure 6-1 Load vs. Deflection Plot for Analytical Models

Table 6-2 Ratio of Predicted Deflections to Branson's Equation

Ratio of Predicted Deflection to Branson's Equation	
Modified Branson	ACI 440.1r-15
1.00	1.00
1.00	1.00
1.00	1.00
1.00	1.00
2.14	1.48
1.98	2.10
1.82	2.03
1.68	1.84
1.55	1.65
1.45	1.50
1.36	1.39
1.30	1.30
1.25	1.23
1.20	1.18
1.17	1.14
1.14	1.11
1.12	1.09
1.10	1.07
1.09	1.06
1.08	1.05
1.07	1.04
1.06	1.03

6.2 Comparison of ANSYS Results to Analytical Results

The ANSYS model should accurately match the experimental results assuming the material properties and modeling techniques were correct. Table 6-3 lists the load vs. deflection values for the model which were determined based on the respective time step.

When comparing the ANSYS to the analytical predicted deflections it is evident the ANSYS model provided the least stiff beam (Figure 6-2). The deflection behavior was consistently greater throughout the loading cycle after the initial crack.

Table 6-3 ANSYS Load (lbs.) vs. Deflection (in.)

ANSYS MODEL	
LOAD	DEFLECTION
0	0.0000
200	0.0002
500	0.0005
1000	0.0011
1200	0.0013
1500	0.0016
2000	0.0021
2500	0.0027
3000	0.0208
4000	0.0331
5000	0.0496
6000	0.0645
7000	0.0768
8000	0.0888
9000	0.1023
10000	0.1157

Figure 6-2 Load vs. Deflection for Analytical and ANSYS Models

6.3   Comparison of Experimental Results to Analytical and Numerical Results

The experimental deflections from Table 4-1 and Table 4-2 were used to calculate the deviations of all the models to each experimental specimen (

Table 6-4). The experimental values were added to the analytical models and shown in Figure 6-3. Up to the first crack moment all of the models reasonably predicted deflection. The analytical models predicted a lower first crack load of approximately 2300 lbs. In comparison, the first crack load for ANSYS model occurred at approximately 2900 lbs. The experimental crack occurred at approximately 3500 lbs. After the first crack significant deviations exist. Branson's equation which equates to the most stiff beam model only over predicted deflection by a factor of 2.97. Although this is significant the modified Branson's equation, ACI 440.1r-15 equation and ANSYS over predicted deflections by a factor of 4.30, 4.48 and 5.30 respectively. After reaching the maximum deviation, all prediction models trended toward converging with the experimental data as the applied load increased. The experimental data suggests the beams were stiffer than anticipated.

Table 6-4 Ratio of Predicted Results to Experimental Results

| Ratio of Predicted Deflection to Experimental Results								
Load	Branson		Modified Branson		ACI 440.1r-15		ANSYS	
	Specimen 1	Specimen 2	Specimen 1	Specimen 2	Specimen 1	Specimen 2	Specimen 1	Specimen 2
1000	0.52	1.05	1.05	1.05	1.05	1.05	1.06	1.06
2000	1.05	1.05	1.05	1.05	1.05	1.05	1.06	1.06
3000	1.97	1.97	3.90	3.90	4.13	4.13	6.93	6.93
4000	2.25	2.43	3.78	4.09	4.15	4.48	4.91	5.30
5000	2.10	2.97	3.04	4.30	3.16	4.46	3.66	5.16
6000	2.18	2.43	2.84	3.16	2.84	3.16	3.22	3.58
7000	1.97	2.70	2.37	2.70	2.33	2.66	2.54	2.89
8000	1.91	2.00	2.18	2.00	2.13	1.95	2.25	2.07
9000	1.77	1.81	1.95	1.81	1.90	1.76	2.01	1.87
10000	1.50	N/A	1.61	N/A	1.57	N/A	1.66	N/A
11000	1.12	N/A	1.18	N/A	1.15	N/A	N/A	N/A
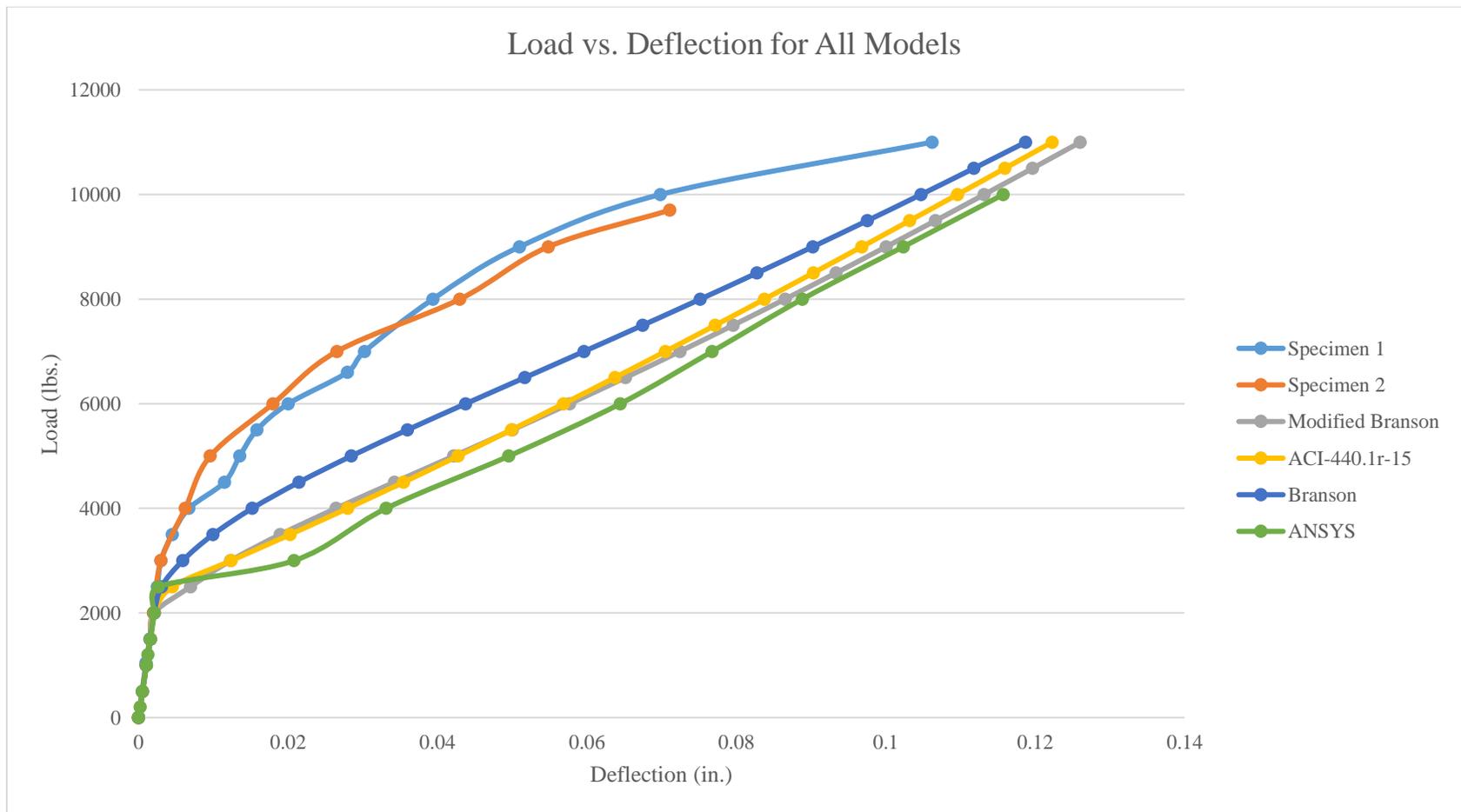
Figure 6-3 Comparison of All Deflection Model

6.4   Possible Reasons for Deflection Discrepancies

The analytical and numerical models are dependent on the material properties. There exists a possibility that the modulus of the reinforcement is higher and/or the concrete compressive and tensile strengths were higher than those observed in the experiments. Manufacturers of FRP materials are encouraged to be conservative on strength values. The specific manufacturer of this product suggested the BFRP rebar may have a tensile modulus up to 10,000 ksi. To check the effect of the stiffer reinforcement on the deflection predictions this value was used for both the analytical and numerical models. The plotted data in Figure 6-4 reflects the deflections assuming the higher tensile modulus of 10,000 ksi. Despite this graph indicating an improvement in deflection predictions compared to the experimental data, Table 6-5 shows significant differences still exist.

Deflections up to first crack match very closely to the ANSYS model. At this point the ANSYS model loses more stiffness than other models. In general Branson's equation is the most accurate. Branson's equation had a maximum overestimation of deflection 2.5 times that of the experimental results. Comparing this overestimation with stiffer reinforcement to the 2.97 times overestimation using manufacturer recommended tensile modulus of 6.7 ksi, there is only an improvement of approximately 20%. This improvement does not justify the large overestimation of deflections for the models.

Since the deflections for the experimental specimens are summations of all previous deflections, any assumed deflection would have an impact on the following measurements. To eliminate the accumulation of 'false' deflections from assuming excessive deflection in the unknown stages up to 3000 lbs. the incremental deflections were tabulated for every 1000 lbs. increment for each load step in Figure 6-5. Analyzing the incremental data shows

there is consistently less deflection in the experimental models when compared to all other models. This would indicate that even with an overestimation of deflection up to 3000 lbs. the beam still exhibited stiffer behavior than expected.

The most probable cause is that the analytical models are empirical and would not reflect the same effect from cracking on the short beam. The small length affected by the curvature and small quantity of cracked sections would result in a stiffer beam than a normal flexural beam that would be more slender and less reinforced. In a longer section, any effect on the curvature from cracked sections is amplified as this slope applies to a greater distance. Additionally, a longer section would have more cracks that contribute to additional deflections along the beam. Both beams only had one major crack up until the load that began to match with incremental deflections of the models in the 6000lb. range. One crack may not have had much of an effect on stiffness and allowed most of the concrete to contribute in tensile resistance which would reduce the overall deflection of the beam. Once the other two cracks developed in the beam additional stresses were being applied to the rebar in multiple locations contributing to additional strain. This strain would reflect as additional deflection. The ANSYS model also considers many more cracks developing than what was observed in the experiments. Considering most of the beams that are modeled have much greater clear span to depth ratios this model may not be acceptable for shorter, deeper beams and/or those that are highly over-reinforced.
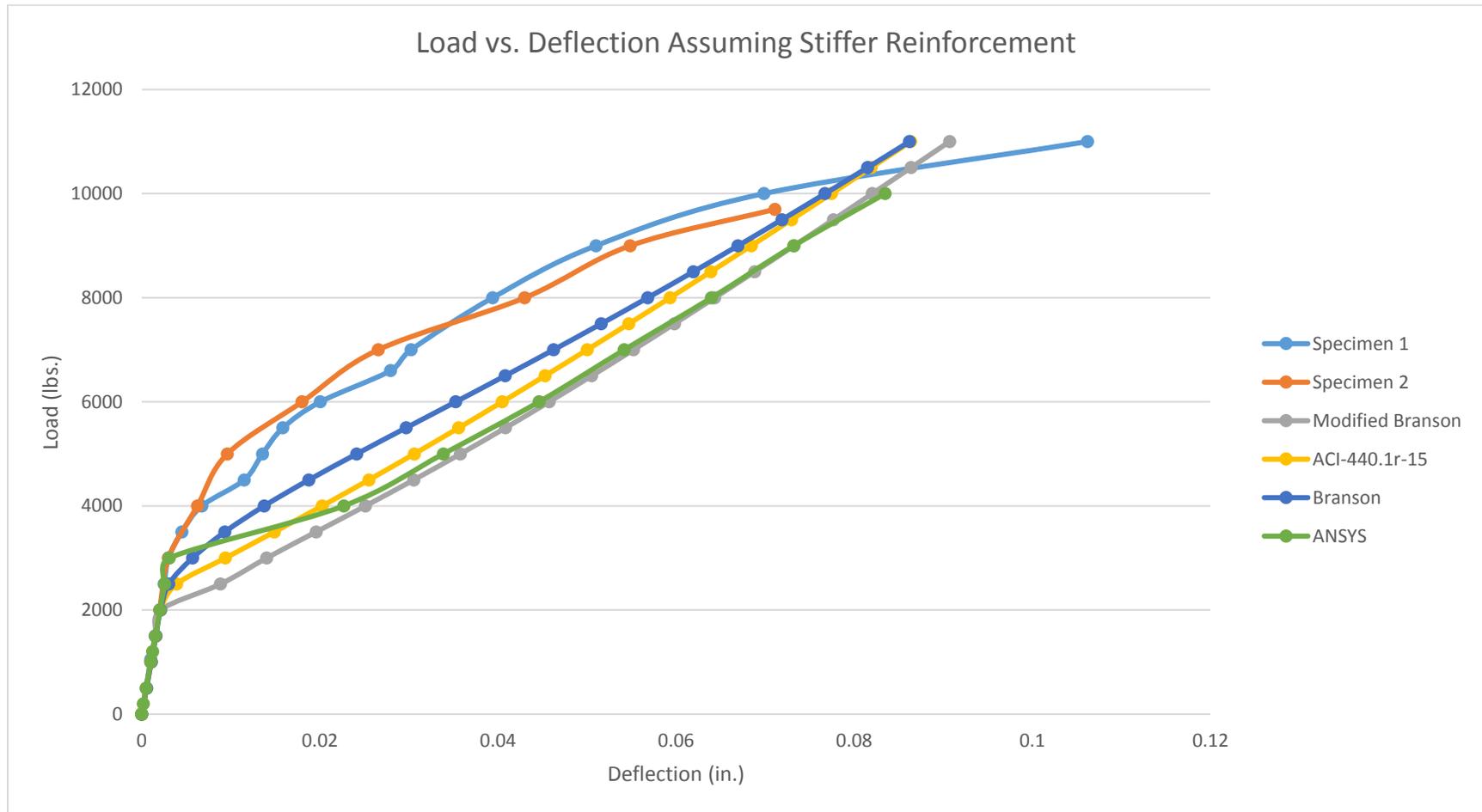
Figure 6-4 All Data Compared When Using Tensile Modulus of 10,000 k

Table 6-5 Ratio of Predicted Results to Experimental Results with Stiffer Reinforcement

Load	Branson		Modified Branson		ACI 440.1r-15		ANSYS	
	Specimen 1	Specimen 2	Specimen 1	Specimen 2	Specimen 1	Specimen 2	Specimen 1	Specimen 2
1000	1.05	1.05	1.05	1.05	1.05	1.05	1.00	1.00
2000	1.05	1.05	1.05	1.05	1.05	1.05	1.02	1.02
3000	1.90	1.90	4.68	4.68	3.13	3.13	1.03	1.03
4000	2.04	2.20	3.72	4.02	3.00	3.24	3.36	3.63
5000	1.78	2.51	2.64	3.73	2.26	3.19	2.50	3.53
6000	1.76	1.96	2.28	2.54	2.02	2.25	2.22	2.48
7000	1.53	1.74	1.83	2.08	1.65	1.88	1.79	2.04
8000	1.44	1.32	1.63	1.50	1.51	1.38	1.62	1.49
9000	1.31	1.22	1.44	1.34	1.34	1.25	1.44	1.33
10000	1.10	N/A	1.17	N/A	1.11	N/A	1.20	N/A
11000	0.81	N/A	0.85	N/A	0.81	N/A	N/A	N/A

Ratio of Predicted Deflection to Experimental Results Assuming BFRP Modulus of Elasticity of 10,000 ksi
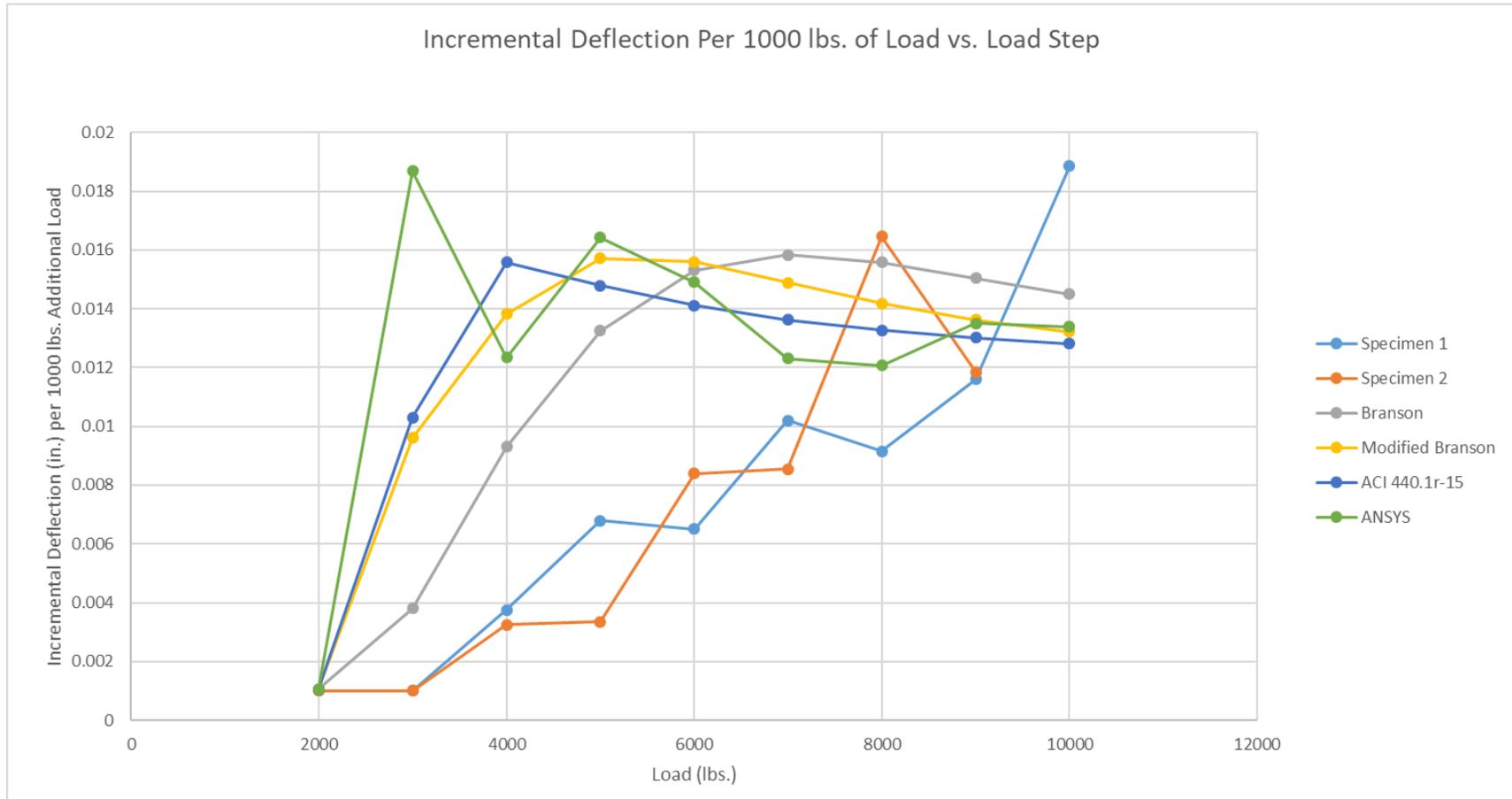
Figure 6-5 Incremental Deflection for 1000 lbs. Incremental at Each Load Step

6.5 Failure Moment

Both experimental beams failed at different ultimate loads. Specimen 1 failed at approximately 11000 lbs. and Specimen 2 failed at approximately 9700 lbs . The ultimate design load was 12550 lbs (Table 6-6). Deviations of specimen 1 and specimen 2 were -12% and -23% when compared to the predicted ultimate load. The differences between both specimens may be attributed to the inconsistency of the concrete between batches. Specimen 2 had more pronounced cracking on one side of the beam with little to no cracking on the other side. This may indicate issues with the concrete that affected the strength properties.

Table 6-6 Predicted and Experimental Failure Load

	P_n (kips)	Deviation
ACI 440.1r-15	12.55	-
Specimen 1	11.00	-12%
Specimen 2	9.70	-23%

7   CONCLUSIONS AND RECOMMENDATIONS FOR FUTURE RESEARCH

This experimental study demonstrated the flexural behavior of two over-reinforced BFRP concrete beams. Despite the limitations of the experimental work, useful data was obtained. The data indicates that short, over-reinforced BFRP concrete beams may not adhere to the behavior of predicted models that may be based on less stiff beams. Even comparisons to Branson's equation which is widely known to overestimate stiffness in FRP reinforced concrete, the experimental specimens proved to be stiffer than this model.

7.1   Recommendations

Performing an experiment that requires such precise and accurate data to the 1000th of an inch requires extremely stringent quality control and assurance through every process. Human error and even deviations in materials can have significant impacts at this level. To limit these issues a longer and less stiff beam design would be an improvement over the short beams tested. It is recommended that future experiments to test the accuracy of current analytical models be performed with a longer, less stiff beam. Larger deflections would reduce the percentage error caused by fractions of an inch in readings. Additionally, the behavior would be more realistic to an actual beam typically used in practice.

Human error is always a limit on the precision and accuracy of an experiment. A few recommendations to prevent this are as follows:

1. Ensure a single batch of concrete can be used for as many specimens as possible with the use of a larger mixer

2.Obtain exact material properties of FRP materials since manufacturers are required to post reduced strengths than what may be used in the experiment

3.Perform experiment with equipment that measures deflection as the load is applied in a single unit or and improved gauge system

It appears that there is justification for research on the deflection behavior of short, over-reinforced FRP beams. Branson's equation did not account for the reduced stiffness of FRP reinforcement because it was an empirical model based on steel reinforced concrete beams which exhibit different stiffness and cracking behaviors. This is what led to the development of the modified Branson equation in ACI 440.1r-06 and eventually the newest equation found in ACI 440.1r-15. All of these equations are empirical to some extent meaning there are limitations to their usefulness based on the experimental data used to develop such equations. Assuming the experimental data is reasonably accurate would necessitate a revised equation for beams that are approaching deep beam behavior. Potential factors to be accounted for should include:

1.Expected   crack pattern

2.Length of region expected to contain a majority of the cracks

3.Reinforcement spacing

4.Significantly over-reinforced members

At this point the current equations overestimate the deflection. This would lead to more conservative designs that are controlled by the serviceability conditions. This does not eliminate the need to provide more accurate information to the practicing engineers.

8   APPENDIX

FINISH

/CLEAR,NOSTART

/FILENAME,BFRPBeam,DB

/TITLE,BEAM

/Prep7

K,1,0,7,0

K,2,0,7,4

K,3,0,0,0

K,4,0,0,4

K,5,34,7,0

K,6,34,7,4

K,7,34,0,0

K,8,34,0,4

V,3,7,8,4,1,5,6,2

ET,1,SOLID65,,,,,

MP,EX,1,4125000

MP,NUXY,1,00.3

TB,CONCR,1

```
TBDATA,1,.5,0.9,542.1,-1

R,1


TB,MISO,MATID,1,8,1

TBPT,,0.00038,1567.5

TBPT,,0.00075,2841.55

TBPT,,0.001,3565.742

TBPT,,0.0015,4578.662

TBPT,,0.002,5080.904

TBPT,,0.002536,5225

TBPT,,0.003,5225

TBPT,,0.0035,5225


VSEL,ALL,,,,

VATT,1,

CM,CONCRETE, VOLU

ESIZE,1,

VMESH,CONCRETE,


K,9,0,1,1

K,10,0,1,3

K,11,34,1,1

K,12,34,1,3
```

```
L,9,11

L,10,12


ET,2,link180

KEYOPT,2,3,1

SECTYPE,1,LINK

SECDATA,0.110447

MP,EX,2,6700000

MP,PRXY,2,00.3


LSEL,NONE,,,,,,,

LSEL,A,,,49

LSEL,A,,,50

CM,FRPRebar,LINE


CMSEL,NONE

CMSEL,S,FRPRebar

LATT,2,,2

LESIZE,ALL,1,,

LMESH,ALL

LPLOT


ET,4,SOLID185

MP,EX,4,29000000

MP,PRXY,4,0.3
```

K,37,18,7,0

K,38,18,7,4

K,39,16,7,4

K,40,16,7,0

K,41,18,8,0

K,42,18,8,4

K,43,16,8,4

K,44,16,8,0

V,37,38,39,40,41,42,43,44

K,45,0,0,0

K,46,0,0,4

K,47,4,0,4

K,48,4,0,0

K,49,0,-3,0

K,50,0,-3,4

K,51,4,-3,4

K,52,4,-3,0

K,53,34,0,0

K,54,34,0,4

K,55,30,0,4

K,56,30,0,0

K,57,34,-3,0

K,58,34,-3,4

K,59,30,-3,4

K,60,30,-3,0

V,45,46,47,48,49,50,51,52

V,53,54,55,56,57,58,59,60

VSEL,S,VOLU,,2,4

CM,PLATE,VOLU

CMSEL,NONE

CMSEL,S,PLATE

VATT,4,,4

ESIZE,1,

VMESH,PLATE

K,13,4,1,1

K,14,4,6,1

K,15,4,1,3

K,16,4,6,3

K,17,7,1,1

K,18,7,6,1

K,19,7,1,3

K,20,7,6,3

K,21,10,1,1

K,22,10,6,1

K,23,10,1,3

K,24,10,6,3

K,25,24,1,1

K,26,24,6,1

K,27,24,1,3

K,28,24,6,3

K,29,27,1,1

K,30,27,6,1

K,31,27,1,3

K,32,27,6,3

K,33,30,1,1

K,34,30,6,1

K,35,30,1,3

K,36,30,6,3

L,13,14

L,13,15

L,15,16

L,14,16

L,17,18

L,17,19

L,19,20

L,18,20

L,21,22

L,21,23

L,23,24

L,22,24

L,25,26

L,25,27

L,27,28

L,26,28

L,29,30

L,29,31

L,31,32

L,30,32

L,33,34

L,33,35

L,35,36

L,34,36

```
LSEL,S,LOC,X,4,10

LSEL,A,LOC,X,24,30

LSEL,A,LOC,Y,1,1

LSEL,U,LOC,X,17

LSEL,U,LOC,Y,0

LSEL,U,LOC,Z,4

LSEL,U,LOC,Z,0

LSEL,U,LOC,Y,-3

CM,SHEAR,LINE

CMSEL,NONE


ET,3,link180

KEYOPT,3,3,1

SECTYPE,2,LINK

SECDATA,0.04909

MP,EX,3,29000000

MP,PRXY,3,00.3


CMSEL,S,SHEAR,LINE

LATT,3,,3

CMSEL,NONE,

CMSEL,S,SHEAR

LESIZE,ALL,1,,

LMESH,ALL

LPLOT
```

```
K,61,0,6,1

K,62,0,6,3

K,63,34,6,1

K,64,34,6,3


L,61,63

L,62,64


LSEL,S,LOC,X,17

LSEL,U,LOC,Y,8,6.5

LSEL,U,LOC,Y,5,-4

CM,COMPRESSIONREBAR,LINE


ET,5,link180

SECTYPE,5,LINK

SECDATA,0.110447

MP,EX,5,6700000

MP,PRXY,5,00.3

CMSEL,NONE

CMSEL,S,COMPRESSIONREBAR,LINE

LATT,5,,5

LESIZE,ALL,1,,

LMESH,ALL

LPLOT


ESEL,S,ENAME,,SOLID65
```

ESEL,A,ENAME,,SOLID185

CEINTF,0.01,

ALLSEL,ALL

ESEL,NONE

ESEL,S,ENAME,,SOLID65

ESEL,A,ENAME,,LINK180

NUMMRG,NODES

NSEL,NONE

NSEL,S,NODE,,1545

NSEL,A,NODE,,1566

NSEL,A,NODE,,1575

NSEL,A,NODE,,1578

NSEL,A,NODE,,1581

D,ALL,UZ,0

D,ALL,UY,0

NSEL,NONE

NSEL,A,NODE,,1645

NSEL,A,NODE,,1666

NSEL,A,NODE,,1675

NSEL,A,NODE,,1678

NSEL,A,NODE,,1681

D,ALL,UY,0

D,ALL,UX,0

```
D,ALL,UZ,0


NSEL,NONE

NSEL,S,NODE,,1492

NSEL,A,NODE,,1497,1500

F,ALL,FY,-2000


ALLSEL,ALL

ANTYPE,STATIC

/TRLCY,ELEM,0.9


/SOLU

TIME, 1500

NSUBST,1500,1500,1500

OUTRES,ALL,ALL

CNVTOL,U,,0.05

CNVTOL,F,,0.005


Solve
```

9 REFERENCES

ACI 2006, Guide for the Design and Construction of Structural Concrete Reinforced with FRP Bars, ACI 440.1R-06, American Concrete Institute, Farmington Hills, MI.2007

ACI 440.1R-15. Guide for the design and construction of concrete reinforced with FRP bars. ACI committee 440. Farmington Hills: American Concrete Institute; 2015.

ANSYS Elem (2015), ANSYS Mechanical APDL Element Reference, ANSYS 15.0, SAS IP, Inc., 2005

ANSYS Theory (2015), ANSYS Mechanical APDL Theory Reference, ANSYS 15.0, SAS IP, Inc., 2005

ASTM C39 / C39M-16b, Standard Test Method for Compressive Strength of Cylindrical Concrete Specimens, ASTM International, West Conshohocken, PA, 2016, www.astm.org

ASTM C78 / C78M-16, Standard Test Method for Flexural Strength of Concrete (Using Simple Beam with Third-Point Loading), ASTM International, West Conshohocken, PA, 2016, www.astm.org

Benmokrane, B.; Chaallal, O.; and Masmoudi, R., 1996, "Flexural Response of Concrete Beams Reinforced with FRP Reinforcing Bars," ACI Structural Journal, V. 93, No. 1, Jan.-Feb., pp. 46-55.

Bischoff, P., 2005, "Reevaluation of Deflection Prediction for Concrete Beams Reinforced with Steel and Fiber Reinforced Polymer Bars," Journal of Structural Engineering V. 131, Issue 5, May 2005

Koch, G.H., Brongers, M.P.H., Thompson, N.G., Virmani, Y.P., Payer, J.H.: Corrosion costsand preventive strategies in the United States, Report no FHWA-RD-01-156,U.S. Departmentof Transportation, Federal Highway Administration, Washington D.C. 2002

Elgabbas, F., Ahmed, E.A., Benmokrane, B., "Physical and mechanical characteristics of new basalt-FRP bars for reinforcing concrete structures." Construction and Building Materials 1 Oct. 2015: 623+. Business Insights: Essentials. Web. 21 Feb. 2017

Elgabbas, F., Vincent, P., Ahmed, E.A., Benmokrane, B., Experimental testing of basalt-fiber-reinforced polymer bars in concrete beams, Composites Part B: Engineering, Volume 91, 15 April 2016, Pages 205-218, ISSN 1359-8368,

Francesca Ceroni, Edoardo Cosenza, Manfredi Gaetano, Marisa Pecce,: Durability issues of FRP rebars in reinforced concrete members, Cement and Concrete Composites, Volume 28, Issue 10, November 2006, Pages 857-868, ISSN 0958-9465

Gao, D.; Benmokrane, B.; and Masmoudi, R., 1998a, "A Calculating Method of Flexural Properties of FRP-Reinforced Concrete Beam: Part 1: Crack Width and Deflection," Technical Report, Department of Civil Engineering, University of Sherbrooke, Sherbrooke, Québec, Canada, 24 pp.

Garbacz, A., Urbanski, M., & Lapko, A. (2013). BFRP bars as an alternative reinforcement of concrete structures - compatibility and adhesion issues. Advanced Materials Research, 1129, 233-241.

Hemmaty, Y. (1998). Modelling of the Shear Force Transferred Between Cracks in Reinforced and Fibre Reinforced Concrete Structures,. Proceedings of the ANSYS Conference,Vol. 1, Pittsburgh, Pennsylvania

Huyse, L., Y. Hemmaty and L.Vandewalle (1994). Finite Element Modeling of Fiber Reinforced Concrete Beams. Proceedings of the ANSYS Conference, Vol. 2,, Pittsburgh, Pennsylvania

Kachlakev, D., T. Miller, S. Yim and K. Chansawat (2001). Finite Element Modeling of Reinforced Concrete Structures Strengthened with FRP Laminates, Civil and Environmental Engineering, DepartmentCalifornia Polytechnic State University, San Luis Obispo

Lapko, A.., Urbanski, M. (2015). Experimental and theoretical analysis of deflections of concrete beams reinforced with basalt rebar, Archives of Civil and Mechanical Engineering, Volume 15, Issue 1, January 2015, Pages 223-230, ISSN 1644-9665,

Nawy, E., and Neuwerth, G., 1977, "Fiberglass Reinforced Concrete Slabs and Beams," Journal of the Structural Division, ASCE, V. 103, No. ST2, pp. 421-440.

Tavarez, F.A., (2001), "Simulation of Behavior of Composite Grid Reinforced Concrete Beams Using Explicit Finite Element Methods," Master's Thesis, University of Wisconsin-Madison, Madison, Wisconsin.

Urbanski, M., Lapko, A., & Suprynowicz, K. (2015). Analysis of the crack propagation process in concrete beams reinforced with BFRP bars using digital image correlation method. Solid State Phenomena, 240, 55-60.

Xiaochun Fan, Mingzhong Zhang, Experimental study on flexural behaviour of inorganic polymer concrete beams reinforced with basalt rebar, Composites Part B: Engineering, Volume 93, 15 May 2016, Pages 174-183, ISSN 1359-8368

Willam, K.J., Warnke, E.D. "Constitutive Model for the Triaxial Behavior of Concrete". Proceedings, International Association for Bridge and Structural Engineering. Vol. 19. ISMES. Bergamo, Italy. p. 174. 1975.

Wolanski, A., (2004), "Flexural Behavior of Reinfrorced and Prestressed Concrete Beams using Finite Element Anlaysis," Master's Thesis, Marquette University, Milwaukee, Wisconsin.

Woraphot Prachasaree, Sitthichai Piriyakootorn, Athawit Sangsrijun, and Suchart Limkatanyu, "Behavior and Performance of GFRP Reinforced Concrete Columns with Various Types of Stirrups," International Journal of Polymer Science, vol. 2015, Article ID 237231, 9 pages, 2015. doi:10.1155/2015/237231

Wu, W. P., 1990, "Thermomechanical Properties of FiberReinforced Plastic (FRP) Bars," PhD dissertation, West Virginia University, Morgantown, W.Va., 292 pp.

Wu Zhishen, Wang Xin, Wu Gang, Advancement of Structural Safety and Sustainability with Basalt Fiber Reinforced Polymers, International Institute for FRP in Construction (IIFC), 13-15 June 2012

Yost, J.; Gross, S.; and Dinehart, D., 2003, "Effective Moment of Inertia for GFRP Reinforced Concrete Beams," ACI Structural Journal, V. 100, No. 6, Nov.-Dec., pp. 732-739.

Zhang, L., Sun, Y., & Xiong, W. (2015). Experimental study on the flexural deflections of concrete beam reinforced with basalt FRP bars. Materials and Structures, 48(10), 3279-3293. doi:http://dx.doi.org/10.1617/s11527-014-0398-0

http://opensees.berkeley.edu/wiki/images/3/32/ReinfSteel2430.png